American Mineralogist, Volume 92, pages 289–308, 2007

Diffusion compensation for argon, hydrogen, lead, and strontium in minerals: Empirical relationships to crystal chemistry

ZI-FU ZHAO AND YONG-FEI ZHENG*

CAS Key Laboratory of Crust-Mantle Materials and Environments, School of Earth and Space Science, University of Science and Technology of China, Hefei 230026, China

ABSTRACT

Inspection of available experimental data reveals log-linear compensation effects between activation energies and pre-exponential factors for Ar, H, Pb, and Sr diffusion in a wide array of minerals. As a result, diffusion of Ar, H, Pb, and Sr converges to the same rates, respectively, at isokinetic temperatures in these minerals. Ionic porosity, *Z*, defined as the fraction of the unit-cell volume in a mineral not occupied by ions, is a measure of atomic packing density in silicate, carbonate, and phosphate minerals. Experimental diffusion parameters exhibit first-order correlations with ionic porosity, which proxies for mean metal-oxygen bond length/strength in minerals. An empirical kinetics-porosity model systematizes Ar, H, Pb, and Sr diffusion in minerals for which experimental diffusion data exist. For Ar and H diffusion, linear correlations are documented between activation energy and total ionic porosity. Combination of these correlations with diffusional compensation effects, which are also documented, yields empirical relationships among elemental diffusivity, total ionic porosity, and temperature. Linear correlations are also observed between experimental diffusion coefficients for Pb and Sr at given temperatures and calculated ionic porosities. For most minerals, the empirical predictions are remarkably consistent with experimental data, which strengthens the link between crystal chemistry and diffusion kinetics.

Keywords: Diffusion kinetics, compensation effect, ionic porosity, crystal chemistry, geochronology, geothermometry, geospeedometry

INTRODUCTION

Theoretical prediction of structural, thermodynamic, and diffusion properties in diverse minerals has been approached by means of atomistic or molecular-dynamics simulation methods (e.g., Catlow and Price 1990; Purton and Catlow 1990; Patel et al. 1991; Wright and Catlow 1994; Vocadlo et al. 1995; Wright et al. 1996; Ita and Cohen 1997; Walker et al. 2003). For example, Wright et al. (1995) presented a method to investigate the diffusion of O and OH-groups in grossular garnet by defining an interatomic potential function to describe the total energy of a system in terms of atomic positions. However, their methodology was not amenable to the calculation of absolute diffusion rates in this phase. Ita and Cohen (1997) conducted first-principles molecular-dynamics simulations for MgO, which predicted the free energy of formation and modeled the motion of Mg and O vacancies, and they calculated diffusion coefficients for MgO in the intrinsic regime, as a function of vacancy concentration. Their theoretical diffusion coefficients were in excellent agreement with experimental values, both for Mg (Van Orman et al. 2003) and O (Yang and Flynn 1994), at corresponding vacancy concentrations. However, this example involves a simple oxide mineral. In contrast, the application of such theoretical models to more-complex minerals is not yet practical, given the current state of our knowledge, and therefore other approaches for predicting diffusion parameters (i.e., the activation energies and pre-exponential factors contained in the Ahrrenius equation) are needed.

During the past three decades, Arrhenius diffusion parameters have been determined experimentally for many diffusing species in a wide variety of minerals (e.g., Freer 1981; Brady 1995; Cole and Chakraborty 2001; Zheng et al. 2003, and references therein). Given the large diffusion data set available from these experimental studies, it is now practical to explore an empirical means of correlating experimental diffusion rates with measurable crystal-chemical parameters. The ultimate goal is to provide a means for predicting diffusion parameters for key elements and/or their ions in geologically important minerals not yet studied in the laboratory. Such empirical relationships have been sought for nearly four decades. One such relationship long recognized in diffusion studies is the so-called "compensation law" (Winchell 1969; Hofmann 1980; Hart 1981; Bejina and Jaoul 1997). Compensation in this context refers to log-linear correlations commonly observed between diffusional activation energy (E) and the pre-exponential factor (D_0), which are related by the Arrhenius diffusivity (D) equation, $D = D_0\exp[-E/RT]$, where R is the gas constant and T is temperature in Kelvins. Such compensation has been observed not only for the same diffusing species in different minerals but also for different diffusants in the same mineral (e.g., Voltaggio 1985). Accordingly, Voltaggio

* E-mail: yfzheng@ustc.edu.cn

(1985) presented a compensation-based approach for estimating Ar and Sr diffusivities in feldspars and sheet silicates, which are accurate to within approximately an order of magnitude. In general, however, the applicability of compensation effects for modeling diffusion depends upon the availability of high-quality experimental data for diffusants and minerals of interest. Moreover, the concept itself rests upon an assumption that the diffusion mechanism is the same for all minerals and diffusants under consideration in a given study (Winchell 1969).

An alternative empirical approach to modeling elemental diffusivity in minerals makes use of a simple and readily calculated parameter known as ionic porosity, *Z*, which is a first-order measure of the mean atomic packing density of a mineral. Dowty (1980) suggested that anion porosity (calculated from the volume of anions in the unit cell), electrostatic site energy, and ionic size all exert strong influences on elemental diffusion rates in oxide and silicate minerals. Indeed, Connolly and Muehlenbachs (1988) observed that the activation energy for O diffusion under dry conditions is proportional to anion porosity for the minerals diopside, melilite, nepheline, olivine, spinel, and zircon as well as rhyolite. Furthermore, Muehlenbachs and Connolly (1991) proposed a simple relationship to predict O-diffusion coefficients (anhydrous conditions) from the anion porosities of anorthite, diopside, forsterite, leucite, melilite, nepheline, perovskite, quartz (and SiO_2 glass), sapphire, spinel, MgO, and αFe_2O_3. Fortier and Giletti (1989) established an empirical model to predict the O-diffusion coefficients already known experimentally for another array of rock-forming silicate minerals under hydrothermal conditions. In particular, they quantified their model using total ionic porosities of the selected minerals, as derived from the sums of anion and cation volumes in their unit cells. Zheng and Fu (1998) then extended this model to predict O diffusivity in minerals from anion porosity under both hydrous and anhydrous conditions, and their prediction for anhydrous O diffusivity in zircon was independently confirmed by the empirical estimate of Peck et al. (2003) from a natural observation. Thus, the empirical kinetics-porosity approach to modeling diffusion properties in minerals has already shown some promise, which encouraged us to seek the additional relationships we present in this study.

Knowledge of Ar, Pb, and Sr diffusion kinetics in rock-forming minerals is of fundamental importance for understanding and constraining thermal histories and cooling rates of geological processes (Dodson 1973; Giletti 1974), as typically inferred from mineral-based geothermometry and thermochronology, respectively. In principle, this knowledge is most applicable where mass transport of atoms like Ar and cations like Fe^{2+}, Mg^{2+}, Pb^{2+}, and Sr^{2+} in key minerals was dominated by volume diffusion, wherein the very concept of closure temperature is most relevant (Dahl 1980, 1996a, 1996b, 1997; Villa 1998, 2006). Likewise, knowledge of H diffusion is significant for interpretation of its exchange kinetics with fluids. Hydrogen is one of the most important elements in the universe, wherein it variably occurs as elemental (H_2), oxidized (H_2O and OH^-), and reduced (CH_4) forms. A vast array of experimental data for Ar, H, Pb, and Sr diffusion in diverse minerals is now available, as summarized in Tables 1 and 2. The very existence of these data not only justifies a systematic search for empirical relationships between diffusion parameters and ionic porosity, but also provides the basis for quantifying any such relationships that are found.

Recent studies indicate that Ar and Pb diffusivities are likely to be systematized in terms of crystal-chemical parameters of minerals. By use of total ionic porosity, Dahl (1996a) predicted variations of Ar and O diffusivities in hornblende and related amphiboles as a function of composition; he also presented two nominally successful field tests of his Ar model (see also Kamber et al. 1995). Likewise, in a $^{40}Ar/^{39}Ar$ study of slowly cooled amphiboles and micas in diverse rocks from the Adirondack Lowlands, New York, Dahl et al. (2004; and references therein) presented thermochronologic data showing that F-phlogopite is more Ar-retentive than OH-biotite, as predicted by Dahl (1996b) from interlayer ionic porosities. Finally, Dahl (1997) developed an empirical crystal-chemical framework to systematize the kinetics of Pb loss and fission-track annealing in U-bearing minerals, and then tested various kinetics-porosity-based predictions against known patterns of mineral behavior.

A more accurate method of calculating total ionic porosity than used in previous studies, which accounts for the different coordination radii of O in minerals, and the recent acquisition of additional experimental diffusion data now permit this promising empirical approach for modeling diffusion kinetics to be developed further. Accordingly, this study begins by characterizing compensation behavior in several geochemically important systems and then incorporates ionic-porosity-based formulations into the observed compensation relations. Empirical relationships are thereby established between Ar, H, Pb, and Sr diffusion coefficients, which are already known experimentally for various minerals, and their calculated anion or total ionic porosities. The extent of agreement observed between empirical and experimental results for Ar, H, Pb, and Sr diffusion strengthens the theoretical link intuitively expected between diffusion kinetics of these elements (and/or their ions, depending on the element) and crystal chemistry of the host minerals.

Relationship between diffusion coefficients and ionic porosity

The process of volume diffusion in crystalline solids is widely considered to obey the Arrhenius law of kinetics, which means that temperature exerts a fundamental control on the magnitude of diffusion parameters, whereas lithostatic and hydrostatic pressures exert secondary influences. The load pressure effect is quantified in terms of the activation volume of diffusion, which equals the volume change accompanying movement of a diffusant from one stable site to an adjacent site. The presence of water can significantly enhance volume-diffusion coefficients, inasmuch as new defects may be created in minerals by reaction between the water molecule and M-O linkages within the structural framework. Otherwise, the other important variable controlling the relative magnitude of volume-diffusion parameters from one mineral to another is crystal structure (e.g., Lasaga 1998; Ganguly 2002).

Empirical, kinetics-porosity relationships for elemental diffusion, as developed in this study, build upon the common observation of linear trends between the ionic porosity (*Z*) of selected minerals and both: (1) the activation energy (*E*), for dif-

fusion of Ar and H; and (2) the logarithm of diffusivity (log$D$), for diffusion of Pb and Sr, at particular temperatures. Dowty (1980) first suggested using anion porosity (Z_A) as a direct measure of the atomic packing density of a mineral. He further postulated that porosity thereby proxies for ionic diffusivity of a given diffusant in a given mineral, such that compact structures tend to inhibit volume diffusion whereas open structures facilitate this process. Thus, first-order correlation is to be expected among ionic porosity, bond strength, element mobility, and structural vacancies in a wide array of minerals.

Vacancies are the means by which most atoms diffuse in crystalline solids. Specifically, atoms or ions move by exchanging sites with vacancies, and there is a linear relationship between vacancy concentration and diffusion coefficient; thus, the presence and mobility of vacancies (and other point defects) in minerals facilitates diffusion therein (e.g., Lasaga 1998; Ganguly 2002). Moreover, the number of atoms jumping from their crystal sites into adjacent vacancies is dependent upon the fraction of vacant sites, and the fraction of atoms adjacent to a vacancy possessing sufficient thermal energy to exceed the activation barrier for migration therein (e.g., Lasaga 1998; Ganguly 2002). Thus, total ionic porosity (Z_T) is potentially useful for modeling diffusion properties in minerals to the extent that it accounts for stoichiometric vacancies therein; however, it cannot account for non-stoichiometric vacancies (Dahl 1996a).

The ionic porosity of a mineral is defined as the percentage of its unit-cell volume not occupied by ions, according to the expression:

$$Z_{A/T} = (1 - V_{A/T}/V_C) \times 100 \quad (1)$$

where $V_{A/T}$ is the volume of anions or total ions in the unit cell, respectively, and V_C is the volume of the unit cell. The volume of ions is calculated from published ionic radii and an assumption of spherical geometry. Calculated from compositional and unit-cell data, $Z_{A/T}$ is a first-order monitor of both metal-oxygen (M-O) bond length and strength (e.g., Dahl 1996a, 1996b, 1997, and references therein). Thus, the smaller the $Z_{A/T}$ value, the closer will be the mean atomic spacing in minerals and thus the stronger will be the average M-O bonds.

As shown in Equation 1, ionic porosity of a mineral is determined from the unit-cell volume and the total volume of ions in the unit cell. Since the volume of the unit cell is accurately known for crystalline minerals with fixed composition and crystal structure, the accuracy of ionic porosity calculated from Equation 1 is determined by the values of ionic radii (r) used in the calculation. Because O is the most abundant element in silicate, carbonate, and phosphate minerals, the choice of its ionic radius is fundamentally important in the calculation of ionic porosity for these minerals. A single radius of 1.36 or 1.38 Å for O^{2-} was used in the calculation of ionic porosity in all previous studies, beginning with Dowty (1980) and Fortier and Giletti (1989), respectively. However, the ionic radius of O varies with its coordination number in the crystal structure of minerals (Shannon and Prewitt 1969), and therefore it is an oversimplification to assume a single value when calculating the ionic porosities of their unit cells (Zheng and Fu 1998).

There are two sets of absolute ionic radii available in literature. One is the traditional set based upon $r(^{VI}O^{2-}) = 1.40$ Å, whereas the other is a set of crystal radii based upon $r(^{VI}O^{2-}) = 1.26$ Å and $r(^{VI}F^{-}) = 1.19$ Å (Shannon and Prewitt 1969; Shannon 1976). The crystal radii differ from the traditional radii only by a constant factor of 0.14 Å. Because the crystal radii correspond more closely to the physical size of ions in a solid (Shannon 1976), they should be used in the calculation of ionic porosities of minerals (Zheng and Fu 1998). Thus, for the minerals considered in this study, ionic porosities have been calculated strictly from the crystal radii, while also incorporating the variable coordination numbers for O as appropriate. The mineral unit-cell volumes needed for the calculations are either taken directly from Smyth and Bish (1988) or computed by use of the cell parameters given in Berry et al. (1983).

Usually, the compensation law is manifested as a linear relationship between activation energy (E) and the pre-exponential factor ($\ln D_0$). Indeed, Winchell (1969) and Winchell and Norman (1969) demonstrated that various diffusing species in silicate glasses showed strong correlations between these parameters. Similar correlations were noted also by Hofmann (1980) for cation diffusion in basalt glass and by Hart (1981) for various diffusing species in feldspar and olivine. Likewise, Bejina and Jaoul (1997) demonstrated that Si diffusion in silicate minerals exhibits a well-defined compensation law. In addition, several perovskite-structured materials with the general formula $ATmO_3$ (A = La, Sr, Ca, Ba; Tm = Mn, Cr, Co, Fe, Ti) exhibit the compensation effect, irrespective of the identity of A-site cations or the presence of stoichiometric vacancies (Berenov et al. 2001). Collectively, these relationships imply that diffusion rates of different species in materials with similar structure, or of a given species in various minerals, tend to converge at an isokinetic temperature (T_{iso}) at which all diffusing species of interest will have the same diffusion coefficients (e.g., Lasaga 1998).

The Arrhenius parameters for Ar, H, Pb, and Sr diffusion in several minerals have been determined experimentally in the laboratory. Table 1 lists the published Arrhenius parameters for Ar, H, and Sr diffusion in these minerals, along with their total ionic porosities as calculated in this study; the experimental Pb diffusion parameters and calculated anion porosities of additional minerals are listed in Table 2. Activation energies for Ar, H, Pb, and Sr diffusion in these minerals vary on the order of tens to hundreds of kJ/mol (Tables 1 and 2). Consequently, the diffusion coefficient for a given element or ion thereof may vary by several orders of magnitude across the fossil temperature ranges embodied within many geological settings.

Figure 1 illustrates the common compensation effects between $\ln D_0$ (in cm^2/s) and E (in KJ/mol) for Ar, H, Pb, and Sr diffusion in minerals. The compensation trends shown in Figure 1 can be represented by linear equations of the general form, $\ln D_0 = (\alpha/R)\cdot E - \beta$:

$$\text{Ar: } \ln D_0 = 0.109(\pm 0.006)E - 25.74(\pm 1.34) \quad (2)$$
$$\text{H: } \ln D_0 = 0.107(\pm 0.007)E - 20.88(\pm 1.07) \quad (3)$$
$$\text{Pb: } \ln D_0 = 0.0758(\pm 0.0038)E - 28.23(\pm 1.65) \quad (4)$$
$$\text{Sr: } \ln D_0 = 0.0732(\pm 0.0040)E - 26.62(\pm 1.44) \quad (5)$$

where R equals 8.314 J/(K·mol). Regressed values of the parameters α/R and β are shown with their 1σ statistical errors

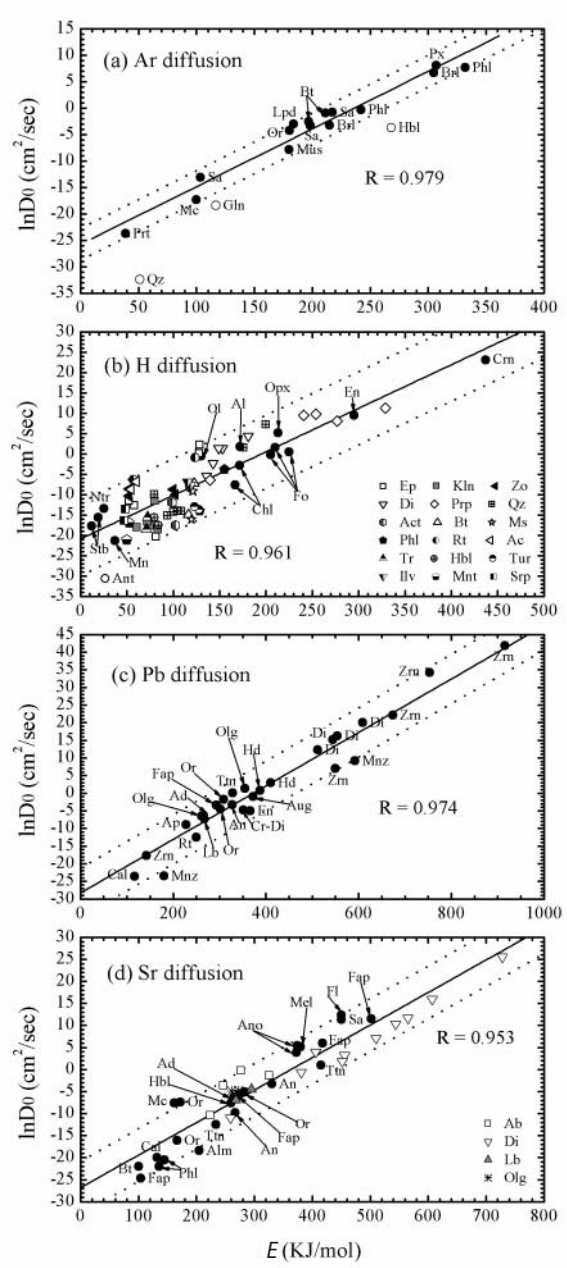

FIGURE 1. Compensation plots of pre-exponential factor ($\ln D_0$) vs. activation energy (E) for diffusion of (**a**) Ar, (**b**) H, (**c**) Pb, and (**d**) Sr, based on experimental diffusion data for selected minerals. No distinction in experimental methods was made between bulk power-fluid exchange and single-crystal diffusion. Solid lines denote best linear fits to the experimental data (Eqs. 2–5), and dotted lines bracket 1σ uncertainties in the regressions. Open circles denote minerals for which diffusion data were not included in the regressions (see the text for explanation). Mineral abbreviations and data references are given in Tables 1 and 2.

in Equations 2–5.

It should be noted that the data available for Ar diffusion in hornblende deviate considerably from the compensation trend (Fig. 1a). These deviations may variably represent an artifact of mineral decomposition during in-vacuo degassing experiments (Gaber et al. 1988) or the fact that hydrothermal experiments may overestimate rates of Ar diffusion in natural settings (Villa et al. 1996), or other unknown factors. Data for Ar diffusion in quartz also deviate significantly from the compensation trend (Fig. 1a), possibly indicating a different mechanism for Ar diffusion than for the other minerals (Watson and Cherniak 2003). Likewise, data for Ar diffusion in glauconite and H diffusion in alunite deviate from the compensation trends (Figs. 1a and 1b). Thus, to at least some extent, scatter in Figure 1 represents the diversity of experimental methodology and conditions, microstructure of starting materials, and (possibly) mechanisms of species transport. Each linear correlation in Figure 1 might have been better, therefore, if all experimental data for the respective diffusant had been produced in the same laboratory, and had the same analytical methodology been applied to both natural and synthetic samples.

As a result of the compensation effect (Fig. 1) for a given diffusant, the Arrhenius functions for all minerals, when plotted as linear trends of log$D$ vs. $1/T$, will tend to intersect at an isokinetic temperature ($T_{iso} = 1/\alpha$). At this unique temperature, all diffusion coefficients are identical for the diffusant, irrespective of the mineral and its ionic porosity. From Equations 2–5, and given that R = 8.314 J/(K·mol), the compensation relations for Ar, H, Pb, and Sr diffusion in the minerals yields calculated isokinetic temperatures of 830, 850, 1310, and 1370 °C, respectively. As pointed out by Lasaga (1998), these results apply to nature only where the isokinetic temperatures closely approximate fossil geological temperatures.

To the extent that diffusivity of an atom or ion is related to the ionic packing densities of minerals, a relationship between diffusivity and ionic porosity is expected at geological temperatures other than T_{iso}. Conceptually, diffusional activation energy is linked to the ionic porosity of a mineral when its M-O bonds are viewed as presenting energy barriers that must be overcome for diffusion to occur. Thus, lower porosity (i.e., shorter M-O bond length) implies a higher energy barrier for diffusion, and vice versa. Indeed, Figure 2 illustrates the expected inverse correlation between activation energy and total ionic porosity, for both Ar and H diffusion in diverse minerals. The strong linear trends shown in Figure 2 can be represented algebraically by the following linear-regressed equations (given with 1σ statistical errors):

$$\text{Ar: } E = -21.44(\pm 2.12)Z_T + 1306.1(\pm 112.3) \quad (6)$$

$$\text{H: } E = -4.00(\pm 0.56)Z_T + 308.9(\pm 30.0) \quad (7)$$

For Ar diffusion, the activation energy inferred at the lowest temperature was used for the linear fitting in cases where more than one set of diffusion data were available for the same mineral (e.g., for biotite, phlogopite, and sanidine, etc.). The reason for this choice is that the experimental results obtained at higher temperatures may correspond to transport effects other than volume diffusion, especially given the tendency toward mineral instability at elevated temperature. On the other hand, processes such as grain-boundary, multipath, or pipe diffusion may become relatively important at lower temperature. Thus, the choice of diffusion coefficients involves appropriate distinction between extrinsic and intrinsic diffusion mechanisms (Lasaga 1998). As noted above, Ar diffusion in quartz may proceed by a different

TABLE 1. Experimental Arrhenius parameters for Ar, H, and Sr diffusion in minerals

Mineral	Abbr.	Z_T	Orientation	T (°C)	P (MPa)	E (kJ/mol)	lnD_0 (cm^2/s)	Reference
Ar diffusion								
Beryl	Brl	58.28	powder	850–950		215 ± 42	–3.22	Vironovskiy (1966)*
Beryl	Brl	58.28	powder	950–1050		305	6.68	Vironovskiy (1966)*
Biotite	Bt	50.15	powder	600–750	100, 1400 "wet"	197 ± 9	–2.56	Harrison et al. (1985)
Biotite	Bt	50.15	powder	550–700	100 "wet"	211.3 ± 5.0	–0.91	Grove and Harrison (1996)
Biotite	Bt	50.15		370	≤200		ln$D$ = –39.78	Villa and Puxeddu (1994)
Glauconite	Gln	54.65	powder	300–600		117	–18.42	Evernden et al. (1960)
Hornblende	Hbl	50.54	powder	750–900	100 "wet"	268.2 ± 7.1	–3.73	Harrison (1981)
Lepidolite	Lpd	48.38	powder	508–602		184	–3.00	Reynolds (1957)
Low sanidine	Sa	55.61	sphere	550–720	0.1–0.2	198.2 ± 10.5	–3.29	Wartho et al. (1999)
Microcline	Mc	55.46		150–400		100	–17.32	Evernden et al. (1960)
Muscovite	Mus	51.50				180	–7.85	Robbins (1972);
Hames and Bowring (1994)								
Orthoclase	Or	53.91	powder	500–800	200	180.3 ± 4.6	–4.27	Foland (1974)
Perthite	Prt	59.63	powder	391–602		39	–23.72	Reynolds (1957)
Phlogopite	Phl	49.70	powder	600–900	100, 200 "wet"	242 ± 11	–0.29	Giletti (1974)
Phlogopite	Phl	49.70	powder	900–1080	1500 "wet"	332	7.69	Giletti and Tullis (1977)
Pyroxene	Px	46.43	powder	650–900		307	8.04	Amikhanff et al. (1959)*
Sanidine	Sa	55.61	powder	390–890		103.3	–13.13	Evernden et al. (1960)
Sanidine	Sa	55.61	powder	500–800		217.4	–0.76	Baadsgaard et al. (1961)
Quartz	Qz	61.62	//c, ⊥c	500–1200	1–185	51.1 ± 6.2	–32.43	Watson and Cherniak (2003)
H diffusion								
Hydroxyl-bearing minerals								
Actinolite	Act	54.08	⊥c	400–700	100	98.75	–11.97	Graham (1981)
Actinolite	Act	54.08	⊥c	400–700	100	118	–8.27	Suzuoki and Epstein (1976)
Actinolite	Act	54.08	//c	400–700	100	102.5	–17.55	Suzuoki and Epstein (1976)
Alunite	Ant		sphere/cyl	100–300	0.1–100	26.4 ± 7.1	–30.62	Stoffregen et al. (1994)
Analcime	Ac	63.75	sphere	65–105	<0.1	60.1	–6.78	Dyer and Molyneux (1968)
Analcime	Ac	63.75	sphere	66–105	<0.1	54.2	–8.72	Dyer and Molyneux (1968)
Biotite	Bt	50.15	//c	450–800	100	116.3	–14.89	Suzuoki and Epstein (1976)
Biotite	Bt	50.15	⊥c	450–800	100	122.6	–7.18	Suzuoki and Epstein (1976)
Chlorite	Chl	56.51	⊥c	500–700	200, 500	171.7	–2.79	Graham et al. (1987)
Chlotite	Chl	56.51	//c	500–700	200, 500	166.9	–7.64	Graham et al. (1987)
Epidote	Ep	45.73	⊥c	200–350	200–400	128	0.21	Graham (1981)
Epidote	Ep	45.73	powder	450–650	200, 400	57.7	–12.62	Graham (1981)
Epidote	Ep	45.73	//c	200–350	200–400	128.5	2.23	Graham (1981)
Epidote	Ep	45.73	//c	450–650	400	52.3	–11.54	Graham (1981)
Epidote	Ep	45.73	//b	200–600	200	81.38	–20.28	De et al. (2000)
Hornblende	Hbl	50.54	//c	350–550	100	79.5	–15.66	Graham et al. (1984)
Hornblende	Hbl	50.54	⊥c	350–550	100	84.1	–17.55	Graham et al. (1984)
Ilvaite	Ilv		⊥c	350–650	9–20	118.5	–7.76	Qian and Guo (1993)
Ilvaite	Ilv		//c	350–650	9–20	115.5	–6.94	Qian and Guo (1993)
Kaolinite	Kln	58.71	⊥c	100, 200	100	60.9	–18.09	O'Neil and Kharaka (1976)
Kaolinite	Kln	58.71	//c	100, 200	100	74.8	–17.66	O'Neil and Kharaka (1976)
Kaolinite	Kln	58.71	//c	200–352	0.032–0.126	83.7	–18.56	Liu and Epstein (1984)
Kaolinite	Kln	58.71	⊥c	200–352	0.032–0.126	72.4	–16.72	Liu and Epstein (1984)
Kaolinite	Kln	58.71	⊥c	150–275	0.03–0.08	80	–11.55	Vennemann et al. (1996)
Manganite	Mn	48.58				37	–21.30	Hariya and Tsutsumi (1981)
Montmor	Mnt	71.28	//c	100, 200	100	49.8	–21.17	O'Neil and Kharaka (1976)
Montmor	Mnt	71.28	⊥c	100, 200	100	52.7	–16.93	O'Neil and Kharaka (1976)
Muscovite	Ms	51.50	//c	450–750	200, 400	119.7	–16.12	Graham (1981)
Muscovite	Ms	51.50	⊥c	450–750	200, 400	121.3	–9.16	Graham (1981)
K-Natrolite	K-Ntr	64.49	sphere	25–65	0.1	25.4	–13.47	Dyer and Faghihian (1998a)
Phlogopite	Phl	49.70	//c	575–650	100	128.6	–14.06	Suzuoki and Epstein (1976)
Phlogopite	Phl	49.70	⊥c	575–650	100	155.2	–3.80	Suzuoki and Epstein (1976)
Serpentine	Srp	57.13	//prism	100–300	200	48.8	–13.59	Sakai and Tsutsumi (1978)
Serpentine	Srp	57.13	⊥prism	100–300	200	47.2	–16.39	Sakai and Tsutsumi (1978)
Na-Stilbite	Na-Stb	70.27	sphere	25–65	0.1	19	–15.63	Dyer and Faghihian (1998b)
Ca-Stilbite	Ca-Stb	70.27	sphere	25–65	0.1	11.8	–17.74	Dyer and Faghihian (1998b)
Tourmaline	Tur	48.40	⊥c	450–800	15–25	127.9	–13.72	Guo and Qian (1997)
Tourmaline	Tur	48.40	//c	450–800	15–25	122.9	–12.98	Guo and Qian (1997)
Tremolite	Tr	52.46	//c	350–800	200–400	72.4	–15.55	Graham et al. (1984)
Tremolite	Tr	52.46	//c	650–850	200–400	71.1	–18.54	Graham et al. (1984)
Zoisite	Zo	45.84	//c	350–650	200–400	100	–8.73	Graham (1981)
Zoisite	Zo	45.84	powder	350–650	200, 400	102.5	–10.02	Graham (1981)
Zoisite	Zo	45.84	⊥c	200–650	200–400	52.3	–10.34	Graham et al. (1980)
Zoisite	Zo	45.84	//c	200–650	200–400	52.3	–8.66	Graham et al. (1980)

* Data cited from Freer (1981).

continued on next page

mechanism than in other minerals, so the experimental result for quartz as determined by Watson and Cherniak (2003) is not used in the linear regression. In addition, because natural quartz may contain fluid inclusions that enhance noble gas retentivity, the experimentally determined diffusion parameters likely represent an end-member case of purely solid-state diffusion (Shuster and Farley 2005). Also, it should be noted that the Ar diffusion data for beryl and lepidolite deviate considerably from those that

TABLE 1. —*Continued*

Mineral	Abbr.	Z_T	Orientation	*T* (°C)	*P* (MPa)	E (kJ/mol)	lnD_0 (cm^2/s)	Reference
Nominally anhydrous minerals								
Adularia	Al	53.91	plate	500–900	0.1	172 ± 15	1.82	Kronenberg et al. (1996)
Corundum	Crn	37.64	//c	1000–1100		437.2	23.06	Ramirez et al. (1997)
Diopside	Di	46.43	//(001), (100), (010)	700–1000	0.1	136 ± 27	–5.39	Ingrin et al. (1995)
Diopside	Di	46.43	//(100)	700–850	0.1	181 ± 38	4.37	Woods et al. (2000)
Diopside	Di	46.43	//(001)	700–850	0.1	153 ± 32	1.38	Woods et al. (2000)
Diopside	Di	46.43	//(001) and (100)	600–900	0.1	149 ± 16	1.38	Hercule and Ingrin (1999)
Diopside	Di	46.43	//(010)	600–900	0.1	143 ± 33	–2.30	Hercule and Ingrin (1999)
Enstatite	En	49.78	//(100) and (010)	700, 900	0.1	295 ± 55	9.52	Stalder and Skogby (2003)
Forsterite	Fo	48.14	//[001]	900–1100	200, 1500 "wet"	210 ± 33	1.61	Demouchy and Mackwell (2003)
Forsterite	Fo	48.14	//[010]	1000–1100	200, 1500 "wet"	205 ± 31	–0.23	Demouchy and Mackwell (2003)
Forsterite	Fo	48.14	//[100]	1000–1100	200, 1500 "wet"	225 ± 40	0.46	Demouchy and Mackwell (2003)
Olivine	Ol	49.60	//a	800–1000	300 "wet"	130 ± 30	–0.51	Mackwell and Kohlstedt (1990)
Orthopyroxene	Opx	51.00	//(001), (100), (010)	700, 1000	0.1	213 ± 47	5.19	Stalder and Skogby (2003)
Pyrope	Prp	39.87		700–950	0.1	254 ± 12	9.78	Wang et al. (1996)
Pyrope	Prp	39.87		700–950	0.1	241 ± 32	9.52	Wang et al. (1996)
Pyrope	Prp	39.87	single crystal	700–950	2700	140±38	–6.45	Blanchard and Ingrin (2004a)
Pyrope	Prp	39.87	single crystal	800–1050	pO_2 = 0.21 atm	277±22	8.06	Blanchard and Ingrin (2004b)
Pyrope	Prp	39.87	single crystal	800–1050	$pO_2 = 10^{-16}$ atm	329±21	11.28	Blanchard and Ingrin (2004b)
β-Quartz	β-Qz	61.62	//c	700–900	890–1550	200 ± 20	7.24	Kronenberg et al. (1986)
α-Quartz	α-Qz	59.89	//c	400–620	2.5	79.5	–9.90	Kats et al. (1962)
β-Quartz	β-Qz	61.62	//c	700–900	2.5	175.7	1.61	Kats et al. (1962)
β-Quartz	β-Qz	61.62	//c	720–850	0.06	93.7	–15.09	Shaffer et al. (1974)
β-Quartz	β-Qz	61.62	//c	721–850	0.06	100	–14.26	Shaffer et al. (1974)
β-Quartz	β-Qz	61.62	//c	722–850	0.06	104.2	–13.91	Shaffer et al. (1974)
β-Quartz	β-Qz	61.62	//c	723–850	0.06	108.4	–13.98	Shaffer et al. (1974)
Rutile	Rt	45.66	//c	614–721	0.1	121 ± 6	–1.27	Johnson et al. (1975)
Rutile	Rt	45.66	⊥c	350–700	0.1	56 ± 2	–6.40	Johnson et al. (1975)
Sr diffusion								
Akermanite	Ak	50.67	//c	1100–1300	0.1	380	5.19	Morioka and Nagasawa (1991)
Albite	Ab	59.63	⊥(001)	675–1025	0.1	224 ± 11	–10.45	Cherniak (1996)
Albite	Ab	59.63	⊥(001)	675–1025	0.1	326 ± 35	–1.32	Cherniak (1996)
Albite	Ab	59.63	//c	640–800	100 "wet"	247 ± 25	–3.68	Giletti (1991)
Albite	Ab	59.63	//c	550–1080	0.1	277 ± 26	–0.21	Giletti and Casserly (1994)
Almandine	Alm	43.15	Isotropic	800–1000	100	205 ± 17	–18.42	Coughlan (1990)
Andesine	Ad	59.65	⊥(001)	725–1075	0.1	265 ± 8	–6.33	Cherniak and Watson (1994)
Anorthite	An	59.68	⊥(010)	725–1075	0.1	330 ± 23	–3.26	Cherniak and Watson (1992)
Anorthite	An	59.68	//c	900–1300	0.1	267 ± 58	–9.77	Giletti and Casserly (1994)
Anorthoclase	Ano	58.49	⊥(001)	725–1075	0.1	374 ±19	5.42	Cherniak and Watson (1992)
Anorthoclase	Ano	58.49	⊥(010)	725–1075	0.1	373 ± 20	3.81	Cherniak and Watson (1992)
Calcite	Cal	62.80	//(1014)	440–800	0.1	132 ± 6	–19.99	Cherniak (1997)
Diopside	Di	46.43	//c	1200–1300	0.1	406 ± 71	3.99	Sneeringer et al. (1984)
Diopside	Di	46.43	//c	1200–1300	0.1	456 ± 75	3.20	Sneeringer et al. (1984)
Diopside	Di	46.43	//a	1150–1250	0.1	452 ± 42	1.86	Sneeringer et al. (1984)
Diopside	Di	46.43	//b	1150–1250	0.1	565 ± 38	11.70	Sneeringer et al. (1984)
Diopside	Di	46.43	//c	1100–1250	0.1	510 ± 29	7.09	Sneeringer et al. (1984)
Diopside	Di	46.43	//c	1100–1250	0.1	544 ± 25	10.34	Sneeringer et al. (1984)
Diopside	Di	46.43	//a	1100–1250	2000	259 ± 50	–10.98	Sneeringer et al. (1984)
Diopside	Di	46.43	//b	1100–1250	2000	381 ± 84	–0.65	Sneeringer et al. (1984)
Diopside	Di	46.43	//c	1100–1250	2000	607 ± 33	15.98	Sneeringer et al. (1984)
Diopside	Di	46.43	//c	1150–1250	1400	728 ± 134	25.51	Sneeringer et al. (1984)
Fluorapatite	Fap	45.06	⊥c	700–1050	0.1	272 ± 9	–5.91	Cherniak and Ryerson (1993)
Fluorapatite	Fap	45.06	⊥c, //c	1050–1250	0.1	418	6.02	Watson et al. (1985)
Fluorapatite	Fap	45.06	//c	650–1000	100 "wet"	104	–24.64	Farver and Giletti (1989)
Fluorapatite	Fap	45.06	//c	1100–1200	100 "wet"	502	11.51	Farver and Giletti (1989)
Fluorite	Fl	46.44	⊥(111)	700–1050	0.1	450±6	12.34	Cherniak et al. (2001)
Hornblende	Hbl	50.54	//c	700–960	200 "wet"	260 ± 12	–7.62	Brabander and Giletti (1995)
Labradorite	Lb	59.66	⊥(001)	725–1075	0.1	268 ± 8	–6.98	Cherniak and Watson (1994)
Labradorite	Lb	59.66	//c	800–1300	0.1	295 ± 31	–4.51	Giletti and Casserly (1994)
Microcline	Mc	55.46	//(010)	800–870	0.1	162	–7.60	Misra and Venkatasubramanian (1977)
Muscovite	Mus	51.50				105	–20.72	Chen et al. (1996)
Oligoclase	Olg	59.64	⊥(001)	725–1075	0.1	273 ± 13	–4.77	Cherniak and Watson (1994)
Oligoclase	Olg	59.64	//c	750–1100	0.1	261 ± 46	–4.91	Giletti and Casserly (1994)
Orthoclase	Or	53.91	//c	625–900	100 "wet"	167 ± 17	–16.12	Giletti (1991)
Orthoclase	Or	53.91	⊥(001)	725–1075	0.1	284 ± 7	–5.12	Cherniak and Watson (1992)
Orthoclase	Or	53.91	//(001)	800–870	0.1	172	–7.42	Misra and Venkatasubramania (1977)
Phlogopite (F-)	F-Phl	50.34	//c	550–1200	0.1	135.9 ± 3.1	–22.03	Hammouda and Cherniak (2000)
Sanidine	Sa	55.61	//(001)	725–1075	0.1	450 ± 13	11.34	Cherniak (1996)
Titanite	Ttn	48.11	//c	700–900	100	234	–12.48	Morishita et al. (1990)
Titanite	Ttn	48.11	//(100)	925–1175	0.1	415 ± 27	0.99	Cherniak (1995b)
Tremolite	Tr	52.46	//c	800	200 "wet"	/	ln$D$ = –38.19	Brabander and Giletti (1995)

* Data cited from Freer (1981).

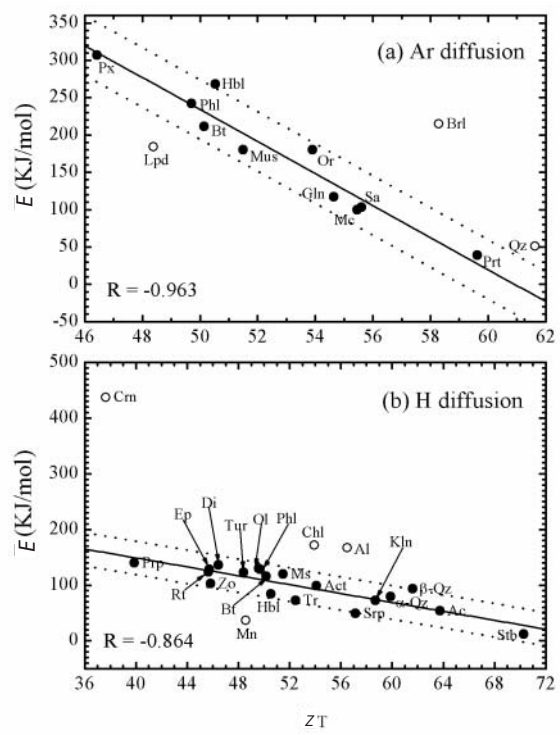

FIGURE 2. Relationships inferred between activation energies (E) for diffusion of (**a**) Ar and (**b**) H in minerals and their total ionic porosities (Z_T). Solid lines denote best linear fits to the experimental data (Eqs. 6 and 7), whereas dotted lines bracket 1σ uncertainties in the regressions. Filled circles represent data that were included in the regressions, whereas open circles denote data that were not included (see text for explanation). Mineral abbreviations, diffusion parameters, and data references are given in Table 1.

are closely correlated for the other minerals, as evident from the overall E-Z_T relationship (Fig. 2a). In summary, except for quartz, beryl, and lepidolite, the remaining minerals including biotite, pyroxene, glauconite, hornblende, micas, and feldspars which represent a range of structures from framework to single-chain silicates, exhibit an inverse, linear correlation between the activation energy for Ar diffusion and total ionic porosity.

For H diffusion, following the practice of Fortier and Giletti (1989), the result corresponding to the fastest rate for H diffusion is used for the linear regression in cases where diffusion rates are anisotropic or where more than one set of diffusion data are available. Furthermore, no distinction was made in Figures 1b and 2b between impurity tracer diffusion in nominally anhydrous minerals and self-diffusion of intrinsic components in hydrous minerals. For the H transport, nevertheless, the volume diffusion through the crystal lattice is the dominant process at high temperatures but the effective diffusion during experimental extraction from or incorporation into crystalline minerals corresponds to the interdiffusion of species with different diffusivities. Data for corundum, adularia, chlorite, and manganite deviate significantly from those of the other minerals in terms of lack of correlation between E and Z_T (Fig. 2b), and thus are arbitrarily excluded from the linear fitting. The reasons for these deviations are not known.

Unlike for the activation energy, the controls on the pre-exponential factor are less understood, and its potential relationship to ionic porosity is likewise less intuitive. As a result, correlations between $\log D_0$ and Z are less apparent than those between E and Z. Assuming, however, that the common compensation effect holds, then Equations 2 and 3 can be combined with Equations 6 and 7 to yield the following empirical relationships between pre-exponential factors and total ionic porosities (with 1σ errors on linear-regressed constants):

TABLE 2. Experimental Arrhenius parameters for Pb diffusion in minerals

Mineral	Abbr.	Z_A	Orientation	T (°C)	P (MPa)	E (kJ/mol)	$\ln D_0$ (cm²/s)	Reference
Andesine	Ad	64.45	⊥(001)	700–1050	0.1	266 ± 12	–6.28	Cherniak (1995a)
Anorthite	An	64.48	⊥(010)	700–1050	0.1	327 ± 11	–3.29	Cherniak (1995a)
Apatite	Ap	60.99	//c	600–900	0.1	228 ± 7	–8.97	Cherniak et al. (1991)
Augite	Aug	57.59	⊥c	850–1050	0.1	372 ± 15	–0.97	Cherniak (2001)
Calcite	Cal	62.80	//[1014]	440–650	0.1	117 ± 9	–23.57	Cherniak (1997)
Diopside	Di	57.01	⊥(110)	800–1100	0.1	544 ± 40	15.21	Cherniak (1998)
Diopside	Di	57.01	⊥(001)	800–1100	0.1	512 ± 23	12.30	Cherniak (1998)
Diopside	Di	57.01	⊥(110)	800–1100	0.1	609 ± 67	20.10	Cherniak (1998)
Cr diopside	Cr-Di	57.01	⊥c	850–1050	0.1	351 ± 36	–4.74	Cherniak (2001)
Enstatite	En	55.44	⊥c	850–1050	0.1	366 ± 29	–5.02	Cherniak (2001)
Fluorapatite	Fap	60.88	⊥c	900–1250	0.1	293	–3.35	Watson et al. (1985)
Hedenbergite	Hd	58.17	⊥(110)	800–1100	0.1	387 ± 31	0.79	Cherniak (1998)
Hedenbergite	Hd	58.17	⊥(110)	800–1100	0.1	410 ± 36	2.94	Cherniak (1998)
Labradorite	Lb	64.46	⊥(001)	700–1050	0.1	267 ± 13	–7.29	Cherniak (1995a)
Microcline	Mc	67.04				89	–12.90	Scott and St-Onge (1995); Rosenqvist (1949)
Monazite	Mnz	55.14	⊥c	1000–1250	0.1	180±48	–23.44	Smith and Giletti (1997)
Monazite	Mnz	55.14	⊥(110)	1100–1350	0.1	592±39	9.15	Cherniak et al. (2004)
Orthoclase	Or	67.01	⊥(001)	700–1050	0.1	309 ± 16	–1.71	Cherniak (1995a)
Orthoclase	Or	67.01	⊥(010)	700–1050	0.1	302 ± 11	–4.58	Cherniak (1995a)
Oligoclase	Olg	64.43	⊥(010)	700–1050	0.1	355 ± 11	1.38	Cherniak (1995a)
Oligoclase	Olg	64.43	⊥(001)	700–1050	0.1	261 ± 13	–6.54	Cherniak (1995a)
Rutile	Rt	51.01	⊥c	700–1100	0.1	250±12	–12.45	Cherniak (2000)
Titanite	Ttn	58.11	//(100)	650–1027	0.1	328 ± 11	0.10	Cherniak (1993)
Zircon	Zrn	53.36		600–1000	0.1	916 ± 88	41.90	Bogolomov (1991)
Zircon	Zrn	53.36		600–1000	0.1	753 ± 75	34.24	Bogolomov (1991)
Zircon	Zrn	53.36		550–800	0.1	142 ± 8	–17.73	Cherniak et al. (1991)
Zircon	Zrn	53.36		900–1100	0.1	674 ± 33	22.09	Lee et al. (1997)
Zircon	Zrn	53.36	//c, ⊥c	1000–1500	0.1, 1000	550 ± 30	7.00	Cherniak and Watson (2001)
Xenotime	Xnt	53.07	⊥(101)	1200–1400	0.1	382 ± 64	–10.43	Cherniak (2006)

$$\text{Ar: } \ln D_0 = -2.34(\pm 0.36)Z_T + 116.62(\pm 18.74) \quad (8)$$
$$\text{H: } \ln D_0 = -0.43(\pm 0.09)Z_T + 12.17(\pm 4.30) \quad (9)$$

The linear relationships in Equations 6–9 can be combined to give additional equations that relate Ar and H diffusivity to temperature and total ionic porosity:

$$\text{Ar: } \log D = (50.64 - 1.02Z_T) - (567.1 - 9.31Z_T)10^3/RT \quad (10)$$
$$\text{H: } \log D = (5.28 - 0.19Z_T) - (134.1 - 1.74Z_T)10^3/RT \quad (11)$$

Total ionic porosities calculated for the minerals of interest in this study, and the corresponding Arrhenius parameters for Ar and H diffusion empirically predicted from Equations 6–9, are presented in Table 3.

From a theoretical perspective, the ionic porosity (Z) may be expected to correlate with migration energy (ME) only. The activation energy (E) represents a combination of the migration energy and the vacancy formation energy (VFE). For example, if the vacancies are of the Schottky-type, then $E = ME + \frac{1}{2} VFE$ (e.g., Ganguly 2002). Thus, where the magnitude of VFE is negligible (or constant) among different mineral systems under consideration, a close correlation between E and ME is expected. Chakraborty et al. (1994) argued that the magnitudes of VFE in silicate minerals are too high relative to measured values of E and, therefore, that diffusion in silicates probably occurs via extrinsic (rather than intrinsic) mechanisms. In that case, a correlation between Z and E is expected, since $VFE = 0$ for an extrinsic mechanism. With a few exceptions, the data in Figure 2 testify to this correlation. Thus, the results summarized in Figure 2 are theoretically reasonable.

A large body of experimental diffusion data are also available for both Pb and Sr in diverse minerals (Tables 1 and 2). Yet, unlike for Ar and H diffusion, linear relationships between E and Z_T for Pb and Sr diffusion are not strong, according to the existing data sets. For Pb diffusion, however, linear trends are evident between diffusion rate and anion porosity at given temperatures. Sr diffusion in Ca-bearing minerals may be dominated by the kinetics of $Sr^{2+} \leftrightarrow Ca^{2+}$ exchange, such that the volume of Ca in the unit cell may influence Sr mobility (especially for calcic minerals such as apatite, fluorite, and calcite). Total ionic porosity (Z_T) is thus used to model Sr diffusion. Figures 3 and 4 illustrate positive, linear correlations between anion porosity (Pb), total ionic porosity (Sr), and Pb and Sr diffusivities in minerals at given temperatures. These relationships can be represented by the following kinetics-porosity equations, expressed as $\log D = A + B \cdot Z_A$ (with 1σ statistical errors for regressed intercepts A and slopes B):

Pb:

$$T = 700\ ^\circ\text{C: } \log D = -70.68(\pm 7.58) + 0.88(\pm 0.13)Z_A \quad (12)$$
$$T = 800\ ^\circ\text{C: } \log D = -62.35(\pm 6.36) + 0.76(\pm 0.11)Z_A \quad (13)$$
$$T = 900\ ^\circ\text{C: } \log D = -55.43(\pm 5.70) + 0.67(\pm 0.10)Z_A \quad (14)$$
$$T = 1000\ ^\circ\text{C: } \log D = -51.52(\pm 5.29) + 0.62(\pm 0.09)Z_A \quad (15)$$

Sr:

$$T = 700\ ^\circ\text{C: } \log D = -33.08(\pm 2.03) + 0.31(\pm 0.04)Z_T \quad (16)$$
$$T = 800\ ^\circ\text{C: } \log D = -29.79(\pm 0.95) + 0.27(\pm 0.02)Z_T \quad (17)$$
$$T = 900\ ^\circ\text{C: } \log D = -27.25(\pm 1.86) + 0.24(\pm 0.04)Z_T \quad (18)$$
$$T = 1000\ ^\circ\text{C: } \log D = -24.08(\pm 2.76) + 0.20(\pm 0.05)Z_T \quad (19)$$

In general, the rate for the fastest transport direction in a mineral or minerals with similar structure and ionic porosity (e.g., plagioclase) is used in cases where diffusion is anisotropic or if multiple sets of data are available. In addition, there are a few other instances in which experimental data are not used in the D-Z or subsequent D-T regressions, as justified below.

Data for Pb diffusion in rutile appear to deviate from the linear trends defined by the other minerals (Fig. 3), but the reason for this behavior is not clear. However, anomalous diffusion behavior has also been observed for O in rutile, as indicated by the observation of faster diffusion at dry conditions than under wet conditions (Moore et al. 1998). Thus, rutile data are plotted in Figure 3 but are not included in the above regressions (Equations 16–19).

Multiple efforts have been undertaken over the past four decades to accurately measure Pb diffusion in zircon, a key mineral in many geochronological studies. Historically, as reviewed by Cherniak and Watson (2003), experimental determinations of Pb diffusivities differ widely among the published studies, such that measured values of D span more than ten orders of magnitude. In some of the experiments (Shestakov 1969, 1972; Magomedov 1970), Pb release did not obey a typical volume-diffusion relationship, indicating the possibility of grain boundary diffusion and suggesting that surface volatilization and Pb migration might have been factors influencing the Pb release patterns. The thermal evaporation experiments of Bogolomov (1991) likely involved decomposition of zircon to $ZrO_2 + SiO_2$ during heating. In this case, therefore, Pb loss was apparently not governed by simple volume diffusion but instead was controlled by the decomposition process and corresponding movement of the reaction front, which greatly enhanced the Pb mobility. The first robust study of Pb diffusion in zircon utilized analytical techniques with superior depth resolution (Cherniak et al. 1991), but their zircon specimen had experienced significant radiation damage in nature, thereby resulting in anomalously high diffusion rates compared with those expected from pristine zircon. Lee et al. (1997) measured out-diffusion of Pb (as well as U and Th) in a natural zircon from Sri Lanka, whereas Cherniak and Watson (2001) conducted Pb-diffusion experiments in zircons encompassing a broad range of experimental conditions and compositions. Different rates of Pb diffusion were inferred in these two studies, in part reflecting differences in both experimental duration and number of data points. Because the Arrhenius equation obtained by Lee et al. (1997) was based on only a few data points (seven points, at only three temperatures) with a modest time series (1.8-fold variation in experimental duration), their results are neither plotted in Figure 3 nor used in the linear regressions. Instead, accepted and thus plotted in Figure 3 are the diffusivity data that Cherniak and Watson (2001) derived from three relatively pristine zircons (both synthetic and natural). Their results were based upon a rigorous time-series experiments (ninefold variation in experimental duration) involving both in- and out-diffusion of Pb, and two different analytical methods [Rutherford backscattering spectrometry (RBS) and electron probe microanalysis (EPMA)]. Because the Arrhenius equation of Cherniak and Watson (2001)

TABLE 3. Empirical diffusivities of Ar, H, Pb, and Sr in minerals as predicted from calculated ionic porosities and published unit-cell data

Mineral	V_A (Å^3)	V_T (Å^3)	V_C (Å^3)	Z_A	Z_T	Ar		H		Pb		Sr	
						E	lnD_0	E	lnD_0	E	lnD_0	E	lnD_0
Anhydrous silicate													
Coesite	237.34	241.76	548.76	56.74	55.94	107	−14.28	85	−11.88	355	−4.39	227	−8.27
Cristobalite	59.34	60.44	172.17	65.54	64.90			49	−15.74	171	−9.45	151	−11.16
β-Quartz	44.50	45.33	118.12	62.30	61.62			62	−14.33	239	−7.59	179	−10.10
α-Quartz	44.50	45.33	113.01	60.62	59.89	22	−23.52	69	−13.58	274	−6.62	194	−9.55
Stishovite	30.41	31.74	46.54	34.66	31.80	624	42.21	182	−1.50	815	8.33	430	−0.49
Tridymite	712.03	725.28	2110.2	66.26	65.63			46	−16.05	156	−9.87	145	−11.40
Albite	237.34	269.32	667.12	64.42	59.63	28	−22.91	70	−13.47	194	−8.81	196	−9.46
Anorthite	474.68	538.82	1336.4	64.48	59.68	27	−23.03	70	−13.49	193	−8.84	195	−9.48
Celsian	474.68	602.27	1466.9	67.64	58.94	42	−21.30	73	−13.17	127	−10.66	202	−9.24
Rb-feldspar	237.34	341.70	736.01	67.75	53.57	158	−8.73	95	−10.87	125	−10.73	247	−7.51
Orthoclase	237.34	331.45	719.13	67.01	53.91	150	−9.53	93	−11.01	140	−10.30	244	−7.62
Sanidine	237.34	320.73	717.15	66.91	55.61	114	−13.51	86	−11.74	142	−10.24	230	−8.17
Kalsilite	59.34	100.16	200.40	70.39	50.02	234	−0.43	109	−9.34	70	−12.25	277	−6.36
Leucite	712.03	966.28	2356.0	69.78	58.99	41	−21.42	73	−13.20	83	−11.89	201	−9.25
Nepheline	237.34	338.82	724.19	67.23	53.21	165	−7.89	96	−10.71	136	−10.43	250	−7.39
Andalusite	152.05	162.22	342.44	55.60	52.63	178	−6.53	98	−10.46	378	−3.73	255	−7.20
Kyanite	153.57	164.79	293.72	47.72	43.90	365	13.89	133	−6.71	543	0.81	328	−4.39
Sillimanite	151.30	159.98	332.29	54.47	51.86	194	−4.73	101	−10.13	402	−3.08	261	−6.96
Akermanite	111.75	151.72	307.55	63.66	50.67	220	−1.95	106	−9.62	210	−8.37	271	−6.57
Beryl	271.46	281.58	674.89	59.78	58.28	57	−19.76	76	−12.89	291	−6.14	207	−9.03
Cordierite	542.92	579.83	1554.77	65.08	62.71			58	−14.80	181	−9.19	170	−10.45
Melilite	111.75	149.29	294.41	62.04	49.29	249	1.28	112	−9.02	244	−7.44	283	−6.13
Acmite	188.54	235.69	429.06	56.06	45.07	340	11.16	129	−7.21	369	−4.00	318	−4.77
Diopside	188.54	234.94	438.58	57.01	46.43	311	7.97	123	−7.79	349	−4.54	307	−5.21
Enstatite	370.99	418.09	832.49	55.44	49.78	239	0.13	110	−9.24	382	−3.64	279	−6.29
Ferrosilite	370.99	418.59	875.85	57.64	52.21	187	−5.55	100	−10.28	336	−4.91	258	−7.07
Hedenbergite	188.54	231.36	450.72	58.17	48.67	263	2.73	114	−8.76	325	−5.21	288	−5.93
Jadeite	188.54	232.62	401.85	53.08	42.11	403	18.08	140	−5.94	431	−2.28	343	−3.81
Omphacite	188.54	233.78	415.10	54.58	43.68	370	14.41	134	−6.61	400	−3.14	330	−4.32
Spodumene	188.49	204.19	389.15	51.56	47.53	287	5.40	119	−8.27	463	−1.40	298	−5.56
Ca-Tschermaks	185.49	219.01	421.35	55.98	48.02	277	4.25	117	−8.48	371	−3.95	294	−5.72
Bustamite	278.24	349.00	764.30	63.60	54.34	141	−10.54	92	−11.20	211	−8.34	240	−7.76
Rhodonite	228.07	327.47	579.84	60.67	43.52	373	14.78	135	−6.54	273	−6.65	331	−4.27
Wollastonite	278.24	356.06	788.04	64.69	54.82	131	−11.66	90	−11.40	189	−8.96	236	−7.91
Almandine	766.31	871.55	1533.2	50.02	43.15	381	15.65	136	−6.38	495	−0.52	335	−4.15
Andradite	766.31	1006.62	1753.2	56.29	42.58	393	16.98	139	−6.14	364	−4.13	339	−3.96
Grossular	766.31	994.36	1661.9	53.89	40.17	445	22.62	148	−5.10	414	−2.75	360	−3.19
Pyrope	766.31	903.12	1504.7	49.07	39.87	451	23.32	149	−4.97	515	0.03	362	−3.09
Spessartine	766.31	916.42	1565.7	51.06	41.47	417	19.58	143	−5.66	473	−1.12	349	−3.61
Uvarovite	766.31	1003.05	1722.8	55.52	41.78	410	18.85	142	−5.80	380	−3.68	346	−3.71
Fayalite	127.72	154.95	307.42	58.45	49.60	243	0.56	111	−9.16	319	−5.37	280	−6.23
Forsterite	127.72	150.17	289.58	55.90	48.14	274	3.97	116	−8.53	372	−3.90	293	−5.76
Kirschsteinite	127.72	166.72	314.89	59.44	47.05	297	6.52	121	−8.06	298	−5.94	302	−5.41
Liebenbergite	127.72	148.01	282.75	54.83	47.65	284	5.12	118	−8.32	395	−3.29	297	−5.60
Monticellite	127.72	164.33	341.84	62.64	51.93	193	−4.90	101	−10.16	232	−7.78	261	−6.98
Tephroite	127.72	159.43	325.02	60.70	50.95	214	−2.60	105	−9.74	272	−6.67	269	−6.66
Hafnon	121.64	144.14	257.60	52.78	44.04	362	13.57	133	−6.77	437	−2.11	327	−4.43
Phenacite	547.36	562.85	1111.6	50.76	49.37	248	1.09	111	−9.06	479	−0.94	282	−6.15
Thorite	121.64	150.30	321.48	62.16	53.25	164	−7.98	96	−10.73	242	−7.51	249	−7.40
Titanite	155.09	192.11	370.23	58.11	48.11	275	4.04	116	−8.52	326	−5.18	293	−5.75
Willemite	547.36	613.56	1577.8	65.31	61.11			64	−14.11	176	−9.32	183	−9.94
Zircon	121.64	138.54	260.80	53.36	46.88	301	6.92	121	−7.99	425	−2.44	303	−5.35
Hydroxyl-bearing silicate													
Anthophyllite	736.00	831.61	1765.8	58.32	52.90	172	−7.17	97	−10.58	322	−5.30	252	−7.29
Cummingtonite	368.00	415.80	902.14	59.21	53.91	150	−9.53	93	−11.01	303	−5.81	244	−7.62
Gedrite	743.60	858.24	1725.7	56.91	50.27	228	−1.01	108	−9.45	351	−4.49	275	−6.44
Glaucophane	368.00	431.66	870.83	57.74	50.43	225	−1.39	107	−9.51	334	−4.96	273	−6.49
Hornblende	371.80	450.14	910.11	59.15	50.54	223	−1.64	107	−9.56	304	−5.77	272	−6.53
Pargasite	368.00	461.14	912.96	59.69	49.49	245	0.81	111	−9.11	293	−6.09	281	−6.19
Riebeckite	372.56	442.69	900.54	58.62	50.84	216	−2.35	106	−9.69	315	−5.47	270	−6.63
Tremolite	368.00	432.42	909.60	59.54	52.46	181	−6.14	99	−10.39	296	−6.00	256	−7.15
Annite	181.80	248.36	506.82	64.13	51.00	213	−2.72	105	−9.76	200	−8.64	268	−6.68
Biotite	181.80	239.87	481.19	62.22	50.15	231	−0.73	108	−9.39	240	−7.54	276	−6.40
Lepidolite	363.60	485.45	940.38	61.33	48.38	269	3.41	115	−8.63	259	−7.03	291	−5.83
Phlogopite	181.80	244.77	486.60	62.64	49.70	241	0.32	110	−9.20	232	−7.78	279	−6.26
Margarite	354.68	395.29	858.59	58.69	53.96	149	−9.65	93	−11.03	314	−5.51	244	−7.63
Muscovite	354.68	452.78	933.56	62.01	51.50	202	−3.89	103	−9.98	245	−7.42	264	−6.84
Paragonite	354.68	396.62	877.51	59.58	54.80	131	−11.61	90	−11.39	295	−6.02	236	−7.90
Amesite	268.62	298.54	688.61	60.99	56.65	92	−15.94	82	−12.19	266	−6.83	221	−8.50
Chlorite	268.62	300.93	691.92	61.18	56.51	95	−15.61	83	−12.13	262	−6.94	222	−8.46

TABLE 3. —*Continued*

Mineral	V_A (Å^3)	V_T (Å^3)	V_C (Å^3)	Z_A	Z_T	Ar		H		Pb		Sr	
						E	lnD_0	E	lnD_0	E	lnD_0	E	lnD_0
Kaolinite	129.94	136.05	329.52	60.57	58.71	47	−20.76	74	−13.08	275	−6.59	203	−9.16
Lizardite	67.16	75.69	178.09	62.29	57.50	73	−17.93	79	−12.56	239	−7.58	214	−8.77
Pyrophyllite	181.80	188.98	425.16	57.24	55.55	115	−13.37	87	−11.72	344	−4.68	230	−8.15
Serpentine	134.31	152.56	355.83	62.26	57.13	81	−17.06	80	−12.40	239	−7.57	217	−8.66
Talc	181.80	199.93	453.77	59.94	55.94	107	−14.28	85	−11.88	288	−6.23	227	−8.27
Axinite	244.16	282.31	566.66	56.91	50.18	230	−0.80	108	−9.41	351	−4.49	275	−6.41
Chloritoid	424.38	472.77	930.08	54.32	49.17	252	1.56	112	−8.97	405	−2.99	284	−6.09
Epidote	202.24	248.93	458.73	55.91	45.73	326	9.61	126	−7.49	372	−3.91	313	−4.98
Humite	438.23	524.41	1014.1	56.79	48.29	271	3.62	116	−8.59	354	−4.42	291	−5.80
Prehnite	181.51	214.56	466.01	61.05	53.96	149	−9.65	93	−11.03	265	−6.87	244	−7.63
Staurolite	368.74	401.21	739.94	50.17	45.78	325	9.49	126	−7.52	492	−0.60	312	−5.00
Topaz	174.29	185.44	346.27	49.67	46.45	310	7.93	123	−7.80	502	−0.32	307	−5.21
Tourmaline	702.77	796.20	1543.1	54.46	48.40	268	3.36	115	−8.64	402	−3.07	290	−5.84
Vesuvianite	1171.0	1557.52	2841.8	58.79	45.19	337	10.88	128	−7.26	312	−5.57	317	−4.81
Zoisite	404.48	489.85	904.47	55.28	45.84	323	9.35	126	−7.54	385	−3.55	312	−5.02
Carbonate													
Ankerite	143.68	172.07	326.63	56.01	47.32	292	5.89	120	−8.18	370	−3.97	299	−5.49
Calcite	136.84	174.65	367.85	62.80	52.52	180	−6.28	99	−10.41	228	−7.88	256	−7.17
Dolomite	143.68	170.28	320.24	55.13	46.83	302	7.04	122	−7.97	388	−3.46	304	−5.33
Magnesite	136.84	152.82	279.05	50.25	45.24	336	10.76	128	−7.28	490	−0.65	317	−4.82
Rhodochrosite	136.84	159.77	307.86	55.55	48.10	275	4.07	117	−8.51	380	−3.70	293	−5.74
Siderite	136.84	156.41	293.17	53.32	46.65	306	7.46	122	−7.89	426	−2.42	305	−5.28
Aragonite	95.79	129.29	226.91	57.79	43.02	384	15.95	137	−6.33	333	−4.99	336	−4.11
Cerussite	95.79	146.85	269.83	64.50	45.58	329	9.96	127	−7.43	193	−8.86	314	−4.93
Strontianite	95.79	140.77	255.13	62.46	44.82	345	11.74	130	−7.10	235	−7.68	321	−4.69
Witherite	95.79	159.37	303.81	68.47	47.54	287	5.38	119	−8.27	110	−11.14	298	−5.56
Phosphate													
Chlorapatite	217.10	299.81	543.01	60.02	44.79	346	11.81	130	−7.09	286	−6.28	321	−4.68
Fluorapatite	204.65	287.36	523.09	60.88	45.06	340	11.18	129	−7.21	268	−6.77	318	−4.76
Hydroxyapatite	206.41	289.12	529.09	60.99	45.36	334	10.48	127	−7.33	266	−6.83	316	−4.86
Monazite ($CePO_4$)	134.00	169.62	298.70	55.14	43.21	380	15.51	136	−6.41	388	−3.47	334	−4.17
Xenotime (YPO_4)	134.00	160.30	285.54	53.07	43.86	366	13.99	133	−6.69	431	−2.27	329	−4.38

Note: Column labels V and Z denote the volume and ionic porosity of unit cell, respectively; subscripts A, C, and *T* denote the anion, cation, and total ion, respectively.

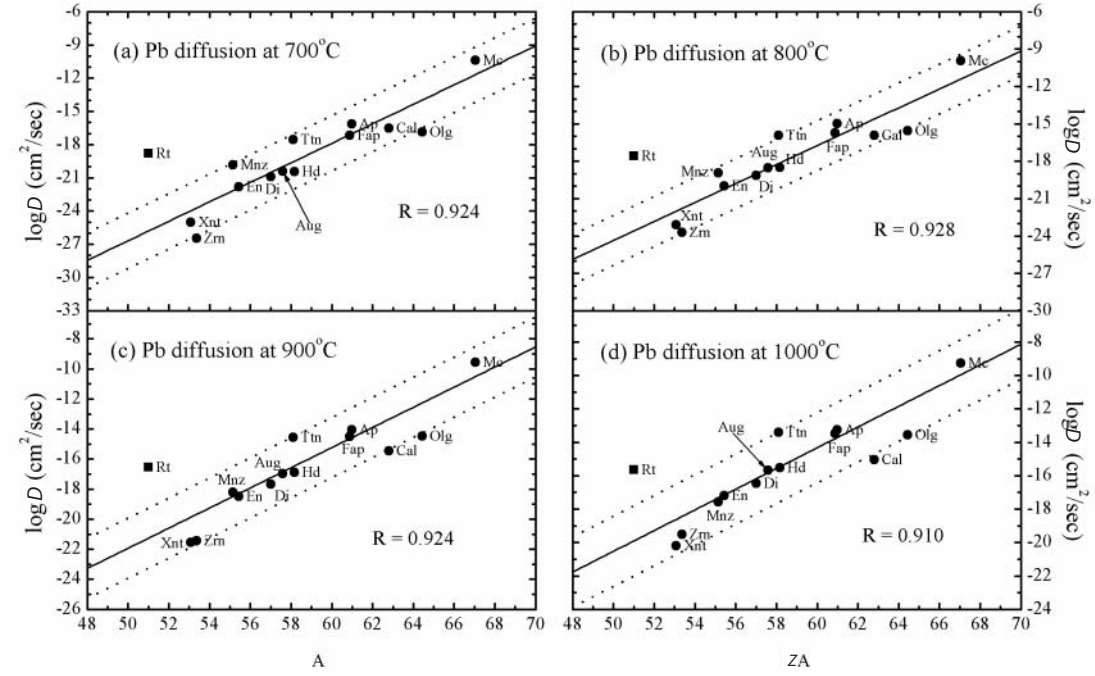

FIGURE 3. Plots of log*D* (diffusivity) for Pb vs. anion porosity (Z_A) in minerals at temperatures of: (**a**) 700, (**b**) 800, (**c**) 900, and (**d**) 1000 °C. Solid lines denote best linear fits to the experimental data (Eqs. 12–15), whereas dotted lines bracket 1σ uncertainties of the regressions. Filled circles represent data that were included in the regressions; solid squares denote data for rutile, which were not included (see text for explanation). Mineral abbreviations, diffusion parameters, and data references are given in Table 2.

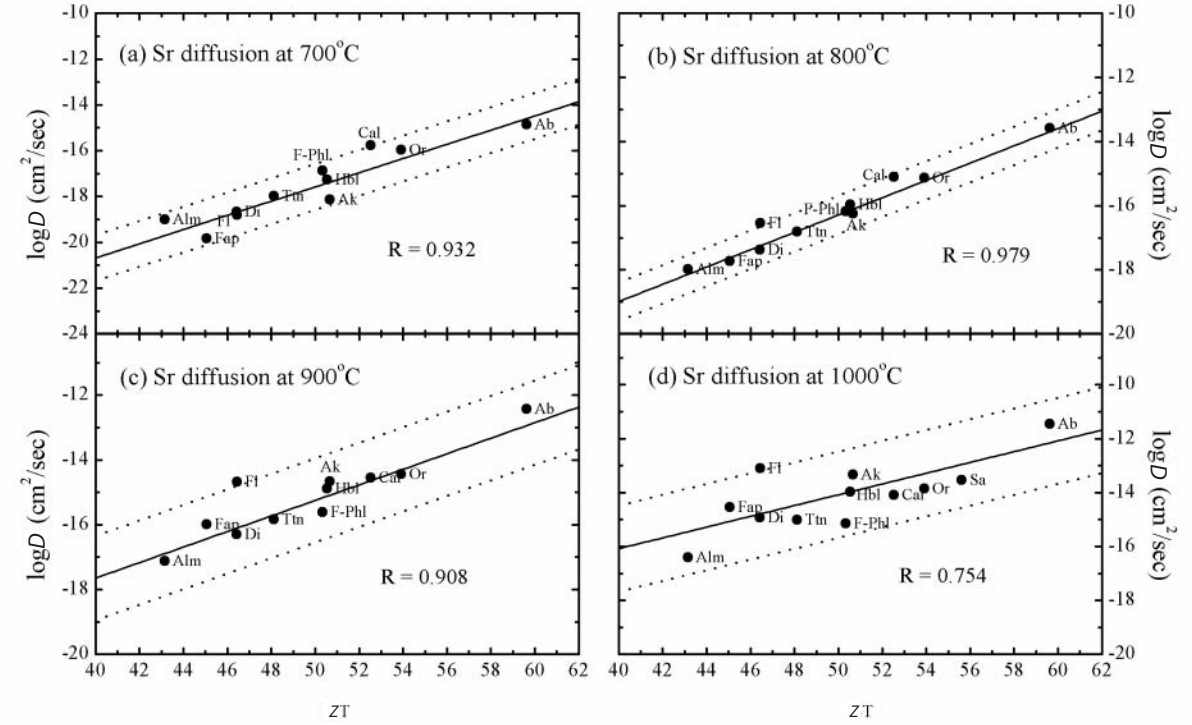

FIGURE 4. Plots of log$D$ (diffusivity) for Sr vs. total ionic porosity (Z_T) in minerals at temperatures of: (**a**) 700, (**b**) 800, (**c**) 900, and (**d**) 1000 °C. Solid lines denote best linear fits to the experimental data (Eqs. 16–19), whereas dotted lines bracket 1σ uncertainties of the regressions. Mineral abbreviations, diffusion parameters, and data references are given in Table 1.

was fitted from experimental zircon data obtained at 1000–1500 °C, a progressive deviation of their data point from the linear trends between log$D$ and Z_A is observed with decreasing temperature, down to 700 °C (Fig. 3).

As outlined in Cherniak and Watson (1992), there are several problems with the experimental results for Sr diffusion in microcline and orthoclase determined by Misra and Venkatasubramanian (1977), which thus are not included in the linear regressions. Likewise, although data for Sr diffusion in sanidine (Or_{61}) at 1000 °C are in good agreement with the linear trend, the results at lower temperatures plot somewhat below the linear trends defined by the other diffusion data (Fig. 4). Finally, as noted by Cherniak (1996), rates of Sr diffusion in alkali feldspar are related to composition at lower temperatures, with diffusivities for intermediate compositions being lower than those for near end-members, but relatively insensitive to composition at high temperatures.

The kinetics-porosity relationships shown in Figures 3 and 4 for Pb and Sr diffusion in minerals are also systematically dependent upon temperature. The diffusivities in diverse minerals obey the Arrhenius relation across the temperature ranges over which they were determined. Therefore, both intercept A and slope B in Equations 12–19 can be expressed as linear functions of $1/T$, as shown in Figures 5 and 6. The algebraic expressions for A and B are thus represented by the following equations (with 1σ statistical errors):

Pb:

$$A = 12.28(\pm 4.03) - 80.37(\pm 4.45) \times (10^3/T) \quad (20)$$

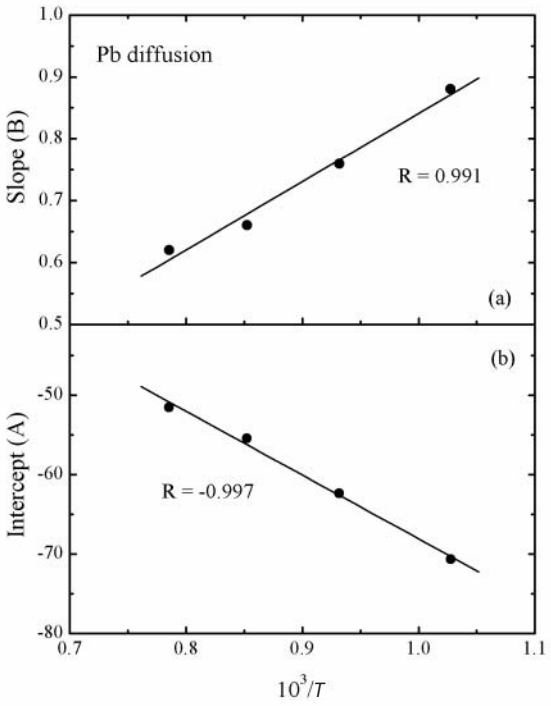

FIGURE 5. Plots of the kinetics-porosity relationships for Pb diffusion in minerals, expressed in the form: log$D$ = A + B·Z_A, where B and A are regressed estimates of slope and intercept, respectively, plotted vs. $10^3/T$. See text for explanation.

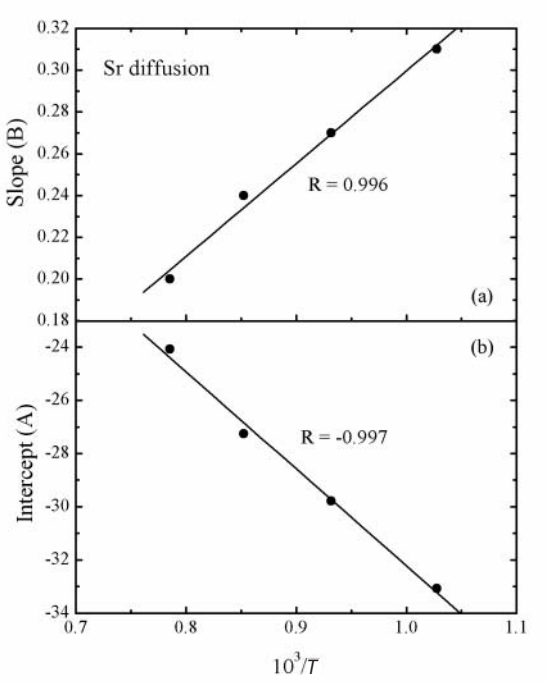

FIGURE 6. Plot of the kinetics-porosity relationship for Sr diffusion, expressed in the form: $\log D = A + B \cdot Z_A$, where B and A are regressed estimates of slope and intercept, respectively, plotted vs. $10^3/T$. See text for explanation.

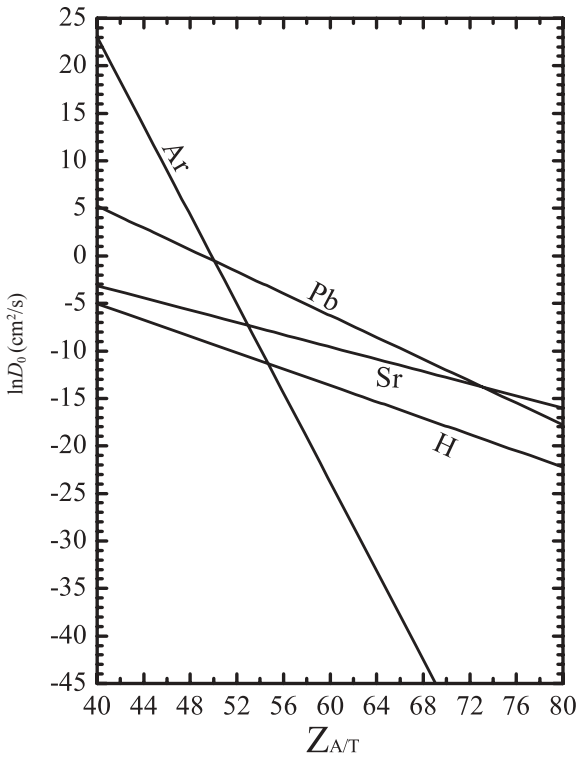

FIGURE 7. The empirical relationship between pre-exponential factor and ionic porosity for Ar, H, Pb, and Sr diffusion in minerals.

$$B = -0.25(\pm 0.07) + 1.09(\pm 0.08) \times (10^3/T) \quad (21)$$

Sr:

$$A = 4.24(\pm 1.92) - 36.46(\pm 2.12) \times (10^3/T) \quad (22)$$

$$B = -0.14(\pm 0.03) + 0.44(\pm 0.03) \times (10^3/T) \quad (23)$$

Combining Equations 12–23 yields the following empirical expressions that correlate diffusivity with both ionic porosity (calculated at standard conditions) and temperature:

$$\text{Pb: } \log D = 12.28 - 80.37 \times 10^3/T + (-0.25 + 1.09 \times 10^3/T) Z_A \quad (24)$$

$$\text{Sr: } \log D = 4.24 - 36.46 \times 10^3/T + (-0.14 + 0.44 \times 10^3/T) Z_T \quad (25)$$

Equations 24 and 25 permit empirical estimation of the corresponding Pb and Sr diffusivities (D) for any temperature and mineral, according to its calculated ionic porosity (Tables 1–3). By first calculating the Pb or Sr diffusivities at different temperatures for a given mineral and constructing a standard Arrhenius plot of $\ln D$ vs. $1/T$, it is then possible to estimate the corresponding diffusional activation energy (slope) and pre-exponential factor (y-intercept), as summarized for many minerals in Table 3.

Figure 7 illustrates the relationships predicted between total ionic porosities and pre-exponential factors for Ar, H, and Sr in diverse minerals, as well as that between anion porosity and pre-exponential factors for Pb in other minerals. These predictions may have some value when experimental data for minerals are lacking (or conflicting). On a cautionary note, however, the uncertainty in Ar, H, Pb, and Sr diffusivities as independently estimated from Equations 10, 11, 24, and 25 and plotted in Figures 8–11, respectively, may be as large as 2–3 orders of magnitude in some cases.

ERROR SOURCES

Zheng and Fu (1998) suggested that uncertainties in empirical kinetics-porosity relationships arise from several sources. These include: (1) analytical errors inherent in experimentally determined diffusivities; (2) assumption of linear compensation effects; (3) uncertainty arising in the calculation of ionic porosity, and its inherent limitations as a proxy for diffusion parameters; and (4) linear regression on a single independent variable. These respective uncertainties are considered in more detail below.

Errors associated with the experimental data of Ar, H, Pb, and Sr diffusion in minerals are the potentially limiting factor in the empirical relationships derived here. First, even the best-quality diffusion data for a given element in a given mineral can yield somewhat different results for the values of E and D_0. These differences arise because of variations in sample composition and purity and the extent to which equilibrium was achieved in the diffusion experiments (Villa 1998; Jaoul and Bejina 2005). Second, because the temperature range of diffusivity measurement is ofte n very narrow, even a small error in the slope (E) of the Arrhenius line propagates a relatively large error in the extrapolated y-intercept ($\ln D_0$). Thus, experimental data sets representing wider temperature ranges than currently available would be highly desirable for constraining the empirical model better. Third, scatter in Figures 1–4 variably represents the di-

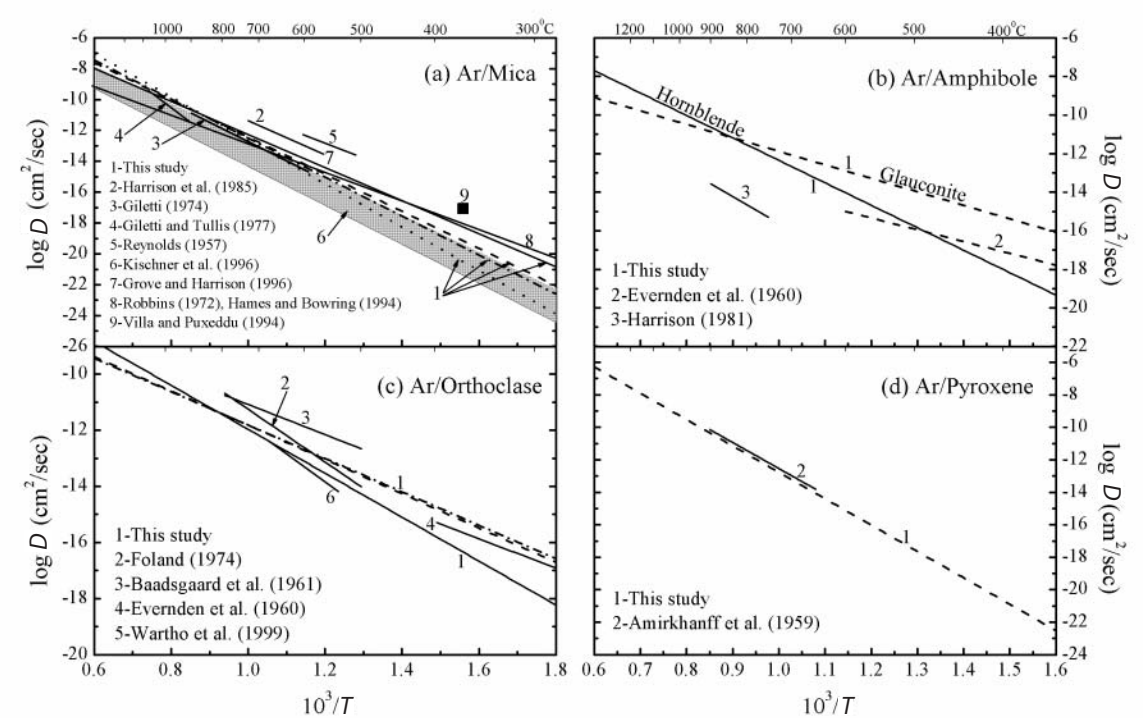

FIGURE 8. Comparison of empirical estimates (this study) with experimental data (Table 1) for Ar diffusivity in minerals: (**a**) mica (dashed line and filled square = biotite, solid line = muscovite, dash-dotted line = phlogopite, dotted line = lepidolite); (**b**) hornblende (averaged composition of Fe- and Mg-hornblende) and glauconite; (**c**) orthoclase (solid line = orthoclase, dash-dotted line = sanidine, dashed line = microcline); (**d**) pyroxene. Additional labels for experimental mica data in **a**: 2,7,9 = biotite; 3,4 = phlogopite; 5 = lepidolite; 6,8 = muscovite.

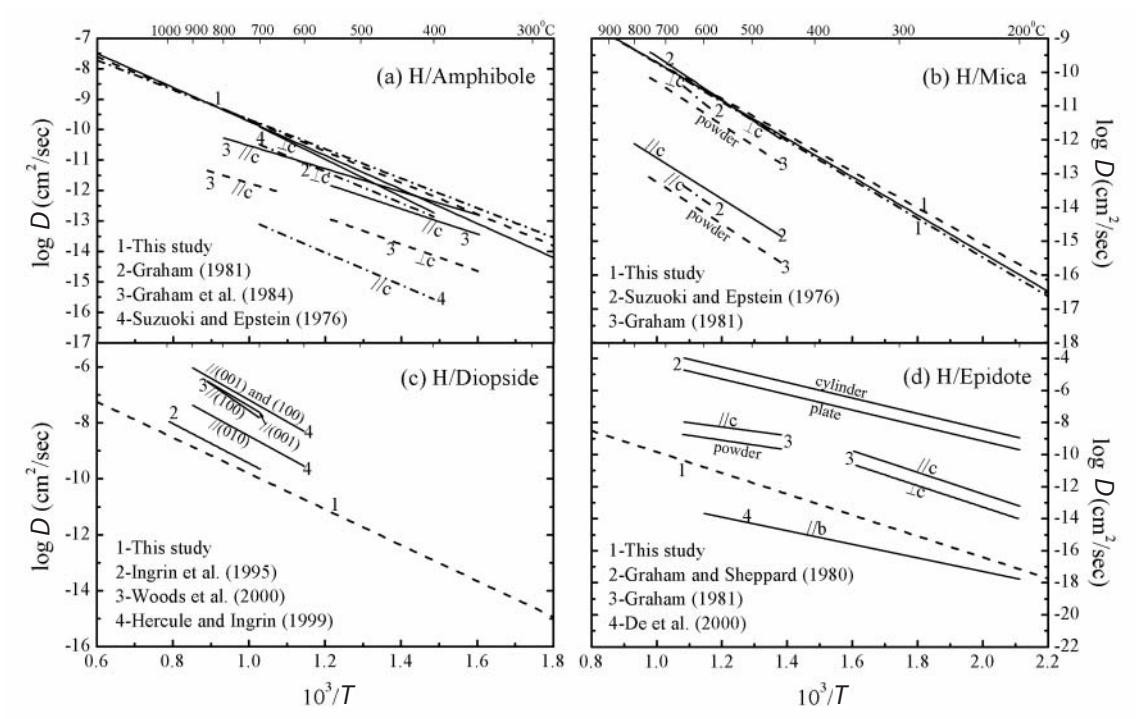

FIGURE 9. Comparison of empirical estimates (this study) with experimental data (Table 1) for H diffusivity in minerals: (**a**) amphibole (solid line = hornblende, dashed line = tremolite, dash-dotted line = actinolite); (**b**) mica (solid line = biotite, dashed line = muscovite, dash-dotted line = phlogopite); (**c**) diopside; (**d**) epidote.

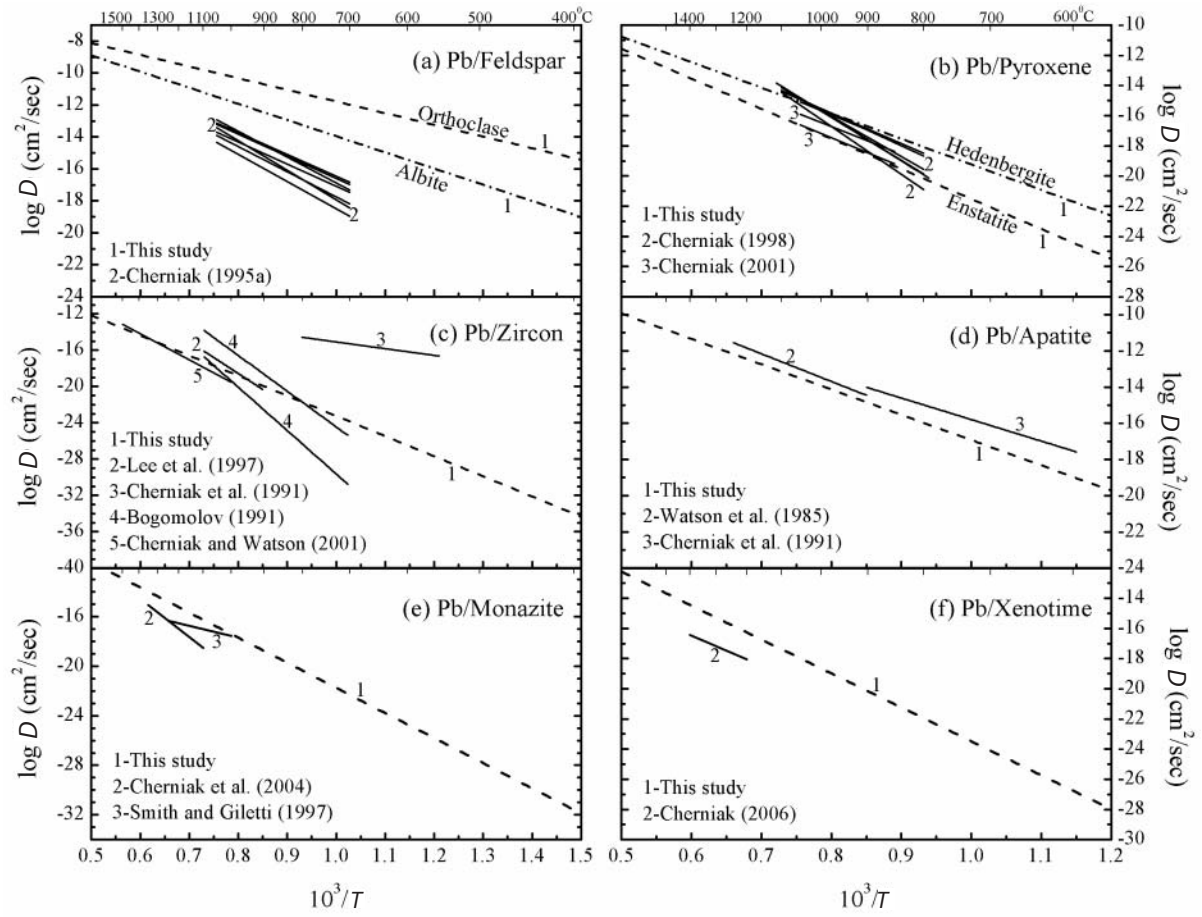

FIGURE 10. Comparison of the empirical estimates (this study) with experimental data (Table 2) for Pb diffusivity in minerals: (**a**) feldspar, (**b**) pyroxene, (**c**) zircon, (**d**) apatite, (**e**) monazite, and (**f**) xenotime.

versity of experimental methodology and conditions, variable microstructures of starting materials, and possibly differing mechanisms of diffusion among minerals (or for a given mineral at different temperatures). Thus, the linear correlations shown in Figures 1–4 might be even tighter if the experimental data were all derived from the same laboratory, with the same analytical technique utilized for both natural and synthetic samples alike.

The diffusional compensation effect between activation energies (E) and pre-exponential factors ($\ln D_0$) rests on the assumption that the diffusion mechanism is the same for a given species in all minerals under consideration (Winchell 1969). The experimental data available for Ar, H, Pb, and Sr diffusion provide robust compensation lines over broad ranges of activation energy (Fig. 1) — i.e., 39–268 kJ/mol (Ar), 12–437 kJ/mol (H), 89–916 kJ/mol (Pb), and 100–728 kJ/mol (Sr). Thus, the requirement of broad ranges in activation energy for compensation relations to be valid (Kemeny and Rosenberg 1973) appears to be met by the experimental data plotted in Figure 1. Therefore, the common compensation trend is assumed to hold for Ar, H, Pb, and Sr diffusion regardless of the diffusion mechansim and medium (dry or wet).

Anisotropy of diffusion within the same minerals does not appear to cause deviation from the compensation relationship. For divalent cations and the anion O^{2-} in minerals such as olivine and diopside, for example, the magnitudes of the diffusion coefficients indicate different E and $\ln D_0$ values in different crystallographic directions (e.g., Zheng et al. 2003). Yet, all couplings of diffusion parameters still fit the compensation line (Fig. 1).

Among isostructural minerals, strong correlation between E and $\ln D_0$ is expected at similar concentrations of cation vacancies and where cation diffusion proceeds by a vacancy mechanism (as is likely for Sr and Pb in most minerals). In a vacancy mechanism, the diffusion coefficient (i.e., the diffusivity, D) is predominantly controlled by the concentration of lattice-site vacancies. In this regard, D_0 is directly proportional to the vacancy concentration, according to the Arrhenius equation, whereas E may be relatively independent of vacancy concentration. Empirical kinetics-porosity relationships are especially well-suited for application to isostructural minerals (e.g., the trioctahedral mica and clinoamphibole groups), where similarity of the O sublattices permits bond length/strengths as proxied by ionic porosity to account for diffusivity differences apparent in nature (e.g., Dahl 1996a, 1996b, 1997). However, deviations from linearity may still arise among naturally occurring isostructural minerals if their vacancy concentrations span many orders of magnitude.

The ionic porosities of selected minerals in this study were calculated from their unit-cell parameters at standard temperature

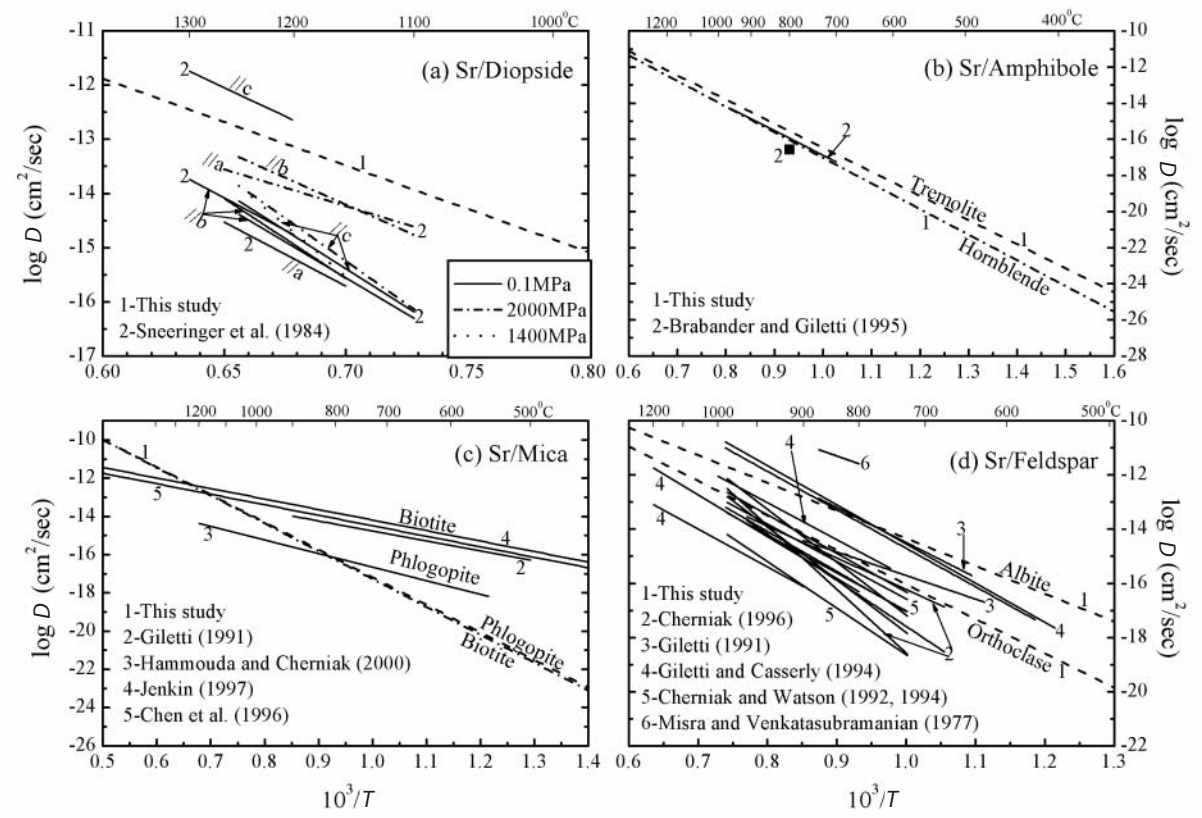

FIGURE 11. Comparison of the empirical estimates (this study) with experimental data (Table 1) for Sr diffusivity in minerals: (**a**) diopside, (**b**) amphibole, (**c**) mica, (**d**) feldspar. Additional labels for experimental feldspar data in **d**: 2,3,4 = albite; 5 = andesine, anorthite, and anorthoclase; 6 = microcline.

and pressure. Thermal expansion and baric compression of the unit cell affects the magnitude of ionic porosity, but only slightly for most minerals. Within the range of crustal temperatures, the thermal expansion of most rock-forming silicates does not exceed 1–2 vol% over the range of geological temperatures (Fortier and Giletti 1989, and references therein). Still, the magnitude of thermal expansion (and thus ionic porosity) varies slightly from mineral to mineral, which propagates as minor uncertainty in diffusional kinetics-porosity models (e.g., Dahl 1996a). Within the range of crustal pressures, the effect of lithostatic pressure on ionic porosity is even smaller (e.g., Dahl 1996b). Thus, *P-T* effects on unit-cell volumes probably introduce minimal error to the empirical kinetics-porosity model presented in this paper, especially as compared with the uncertainties inherent in the experimental results also applied therein.

Linear regressions on a single variable have been used to fit the apparently linear correlations inferred in Figures 1–4, although considerable scatter is still observed. Moreover, the statistical uncertainty associated with the regression intercept is typically larger than that associated with the slope. These uncertainties include not only the systematic and random errors embodied within the experimental data sets but also the shortcomings inherent in basing an empirical diffusion model upon a single independent variable (ionic porosity) instead of on multiple variables. Conceivably, therefore, the model could be enhanced with incorporation of additional independent variables, such as load pressures and fugacities of O and H_2O, as recast into multiple-linear or non-linear regression equations. This goal remains for future work.

Finally, elemental and ionic diffusivities are related to the structural (e.g., imperfections, defects, non-stoichiometry, order-disorder, interatomic potentials) and dynamical (e.g., vibrational spectra, heat capacities) properties of crystalline solids (e.g., Lasaga 1998; Ganguly 2002). The existence of kinetics-porosity relationships for Ar, H, Pb, and Sr diffusion in a variety of crystalline minerals, nevertheless, suggests that diffusion species of molecular and atomic form plays a predominant role on their transport rates within the open space. Only a subordinate control was exerted by those diffusion species bound in the crystal framework, which depends on bond strengths, coordination number, and other structural factors. However, modeling the effects of these properties requires a more sophisticated approach than the relatively straightforward bond-length/strength approach advanced in this paper. Yet the collective influence of these additional mineral properties almost certainly contributes to the scatter observed in Figures 1–4.

COMPARISON WITH KNOWN DATA

To test the validity of the diffusional kinetics-porosity relationships derived in this study, we compare our empirically inferred diffusivities with those determined experimentally by other researchers. The results of these comparisons are summarized

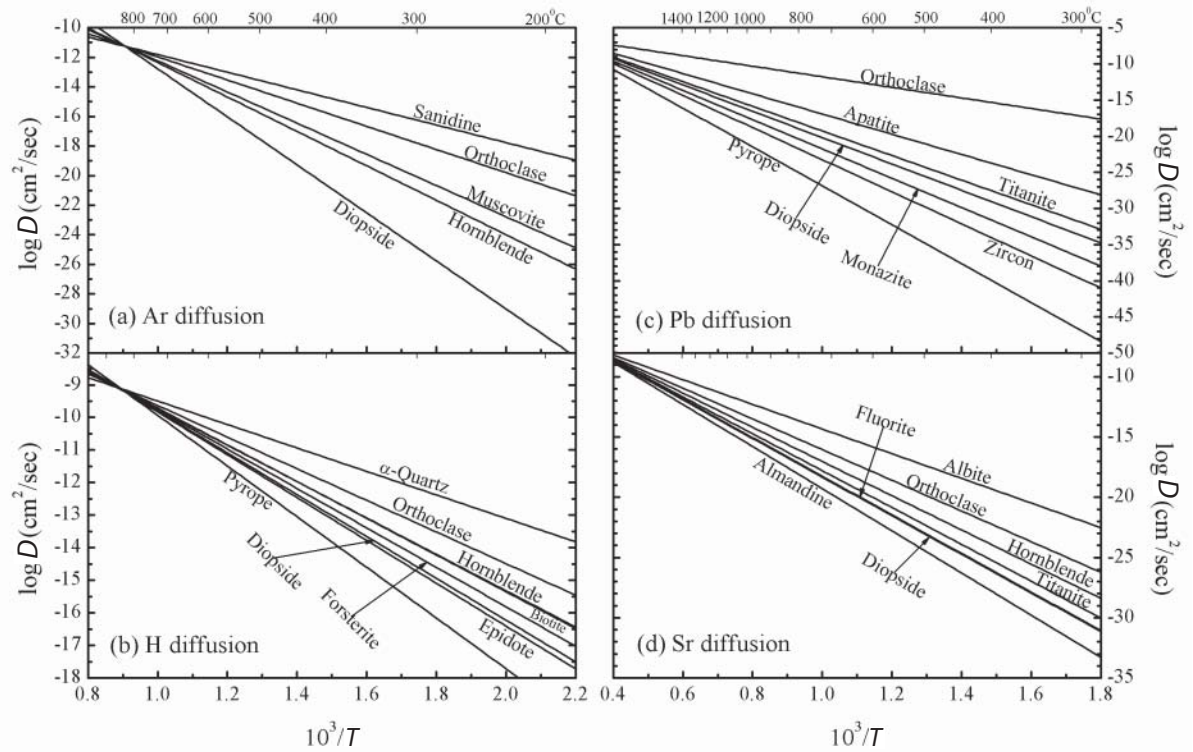

FIGURE 12. Arrhenius plots of empirically estimated diffusivities (Table 3) of various elements in common minerals: (**a**) Ar, (**b**) H, (**c**) Pb, (**d**) Sr.

in Figures 8–11 for diffusion of Ar, H, Pb, and Sr, respectively, in silicate and phosphate minerals.

Figure 8 compares our empirical estimates with the known experimental results for Ar diffusion in mica, hornblende, glauconite, orthoclase, and pyroxene. Our empirical model provides first-order approximations of experimental diffusivities for Ar in micas (biotite, lepidolite, muscovite, and phlogopite), orthoclase, and diopside (Figs. 8a, 8c, and 8d). For Ar diffusion in muscovite, Kischner et al. (1996) empirically inferred activation energies of 230–242 KJ/mol and pre-exponential factors of 0.02–0.24 cm^2/s. By comparison, our respective E and D_0 estimates are 202 KJ/mol and 0.02 cm^2/s, which are equivalent within 1σ uncertainties. Likewise, the parallelism of empirical and experimental slopes for both glauconite and average hornblende in Figure 8b indicates close agreement in the empirical and experimental activation energies for the two amphiboles. On the other hand, the experimental pre-exponential factors for Ar diffusion in glauconite and hornblende not only deviate from the compensation line (Fig. 1a) but also disagree with our empirical estimates (i.e., note disparate y-intercepts in Fig. 8b). However, Wartho et al. (1999) showed that the hornblende Harrison (1981) used for his experiments was somewhat altered by a K-bearing phase, such that the measured diffusion data do not adequately describe the hornblende host per se, which may account for the deviation as observed in Figure 8b.

Figure 9 compares our empirical estimates and the experimental results for H diffusion in amphibole, mica, diopside, and epidote. The empirical estimates are close to the experimental results for actinolite with the diffusion direction normal to the **c**-axis (Fig. 9a), and for hornblende with the diffusion direction parallel to the **c**-axis. The experimental results for tremolite obtained at relatively lower temperatures better match the empirical estimates than those at higher temperatures. The empirical estimates for H diffusion in mica agree well with the experimental results obtained in the direction normal to the **c**-axis, but are significantly larger than the results acquired in the direction parallel to the **c**-axis (Fig. 9b). As illustrated in Figure 9c for diopside, our empirical estimates are very close to the experimental results of Ingrin et al. (1995), but one to four orders of magnitude lower than the experimental results of Hercule and Ingrin (1999) and Woods et al. (2000). The activation energies are quite similar among these results (Figs. 9a–9c), despite some disagreements in diffusivity. Experimental H diffusivities in epidote are not comparable to each other (Fig. 9d), and our empirical estimate is close only to the experimental data of De et al. (2000) at low temperatures.

Figure 10 compares our empirical estimates and the experimental results for Pb diffusion in feldspar, pyroxene, zircon, apatite, monazite, and xenotime. Pb^{2+} diffusion in feldspar is thought to be rate-limited by diffusion of Ca^{2+}, Al^{3+}, and Si^{4+} (Cherniak 1995a), which could overshadow any Z-related effects on Pb diffusivity in feldspar. This consideration may account for the disagreement between the empirical estimates and the experimental results for Pb diffusion in feldspar (Fig. 10a). Nevertheless, the empirical estimates of Pb diffusivity in pyroxene are in fair agreement with the experimental results (Fig. 10b). Moreover, as illustrated in Figure 10c, the empirical estimate for Pb diffusion in zircon is very close to the experimental results of Lee et al. (1997) and Cherniak and Watson (2001). Although the empirical result closely matches the experimental data of Bogolomov (1991) at

experimental temperatures, the relatively high activation energy obtained in his thermal evaporation experiments most likely corresponds to decomposition of zircon rather than volume diffusion per se. Cherniak and Watson (2001) suggested that the results of Cherniak et al. (1991) provided a determination of Pb transport rates in zircons that have experienced significant radiation damage. Indeed, the magnitude of Pb diffusivity in the compromised zircon is significantly greater than our empirical estimate and the other experimental results (Fig. 10c), which describe relatively pristine zircon. The experimental results of Watson et al. (1985) and Cherniak et al. (1991) for Pb diffusion in apatite agree well with the empirical estimates (Fig. 10d). Although the experimental results of Smith and Giletti (1997) and Cherniak et al. (2004) for Pb diffusions in monazite are significantly different in both pre-exponential factor (D_0) and activation energy (E) (Table 2), they are close to the empirical estimate for monazite at the experimental temperatures (Fig. 10e). To some extent, these differences may reflect compositional effects on monazite diffusion parameters, as modeled by Dahl (1997). As depicted in Figure 10f, the experimental result of Cherniak (2006) for Pb diffusion in xenotime is matched by the empirical activation energy (same slopes), but not by the empirical pre-exponential factor (different y-intercepts). As a result, rates of Pb diffusion in xenotime derived from the empirical estimate are faster than those from the experimental determination.

Figure 11 compares our empirical estimates and the experimental results for Sr diffusion in diopside, amphibole, mica, and orthoclase. As shown in Figure 11a, the experimental diffusivity for Sr diffusion in diopside is dependent upon crystallographic direction and pressure. Within experimental uncertainties, the empirical estimates are close to the results obtained at 2.0 GPa pressure and in directions parallel to the **a**- and **b**-axes, as well as at 0.1 MPa and in the direction parallel to the **c**-axis. The empirical estimates for Sr diffusion in amphibole are in good agreement with the experimental results of Brabander and Giletti (1995) (Fig. 11b). The empirical estimates for Sr diffusion in mica are close to the results of Hammouda and Cherniak (2000) at the experimental temperatures as well as to the empirical results of Jenkin (1997) and Chen et al. (1996) at higher temperatures. However, they are lower than the preliminary results of Giletti (1991) and the empirical results of Jenkin (1997) and Chen et al. (1996) at lower temperatures (Fig. 11c). These limited temperature intervals of agreement in diffusivities reflect strong deviations between the empirical and experimental activation energies (cf. slopes). As shown in Figure 11d, the empirical estimates of Sr diffusivities for feldspar, and in particular the activation energies, reasonably approximate the laboratory results of Giletti (1991), Giletti and Casserly (1994), and Cherniak (1996). However, these estimates lie between the experimental results of Misra and Venkatasubramanian (1977) and Cherniak and Watson (1992, 1994).

Finally, Figure 12 depicts the empirical relationships between diffusivities for Ar, H, Pb, and Sr (this study) in various minerals as Arrhenian functions of temperature. The compensation effect results in an intersection of the Arrhenius lines with each other at a single value of the diffusion coefficients at an isokinetic temperature, which is 830, 850, 1310, and 1370 °C for Ar, H, Pb, and Sr diffusion, respectively. On the basis of these trends, the inferred diffusion rates are also systematized by inverse relationships to ionic porosities of the respective minerals. Listed from high to low, the porosity-predicted sequences of diffusivity are as follows:

(1) Ar: sanidine > orthoclase > muscovite > hornblende > diopside;

(2) H: quartz > orthoclase > hornblende > biotite > forsterite > diopside > epidote > pyrope;

(3) Pb: orthoclase > apatite > titanite > diopside > monazite > zircon > pyrope;

(4) Sr: albite > orthoclase > hornblende > titanite > fluorite ≥diopside > almandine.

In a volume-diffusion model of mass transfer in minerals, compact structures (lower Z) are viewed as promoting slower diffusion rates and thus higher closure temperatures, for a given element/ion in a given mineral, whereas the opposite is true for more open structures under the same conditions. In terms of applicability of our model to nature, however, it is important to emphasize that mass transfer by volume diffusion constitutes a fundamental assumption of thermochronology as widely practiced. Nonetheless, to the extent that mean M-O bond length is also rate-limiting with respect to other geologically relevant mechanisms of mass transfer, they will all tend to exhibit parallel kinetic behavior, in a relative sense, from mineral to mineral. That is, a high-porosity mineral may be as susceptible to mass transport of a key atom or ion by volume diffusion as by fluid-driven alteration or metamorphic recrystallization, and vice-versa for low-porosity minerals. To a first approximation, this parallel behavior is manifested in nature by the minerals tending to preserve the same relative age sequence irrespective of the actual mass-transfer process that occurred in a particular geologic setting (e.g., Dahl 1996a, 1996b, 1997; Villa 1998, 2006).

The great success of vacancy mechanisms for diffusion in many solids, such metals and alkali halides, led to the idea that element transport in glass was by ions jumping into ion vacancies. However, it is now generally agreed that O can be transported through crystalline minerals, silicate glasses, and melts by dissolved water molecules and hydroxyl groups. This is essentially implicated by the kinetics-porosity relationships for O diffusion in a variety of crystalline minerals under both wet and dry conditions (Zheng and Fu 1998). It can be understood with the diffusion-reaction and exchange mechanism of molecular H_2O and ionic OH, which dissolve and diffuse in the open mineral structure and in which O atoms can exchange with the O atoms in the cation-oxygen bonds. Likewise, diffusion of molecular and atomic species is also implicated by the kinetics-porosity relationships for Ar, H, Pb, and Sr diffusion in various crystalline minerals. In this regard, Ar can be transported through the minerals by molecular Ar, H by molecular H_2O (possibly also by ionic OH^-, H_3O^-, and/or H^+), and Pb and Sr by monoxides PbO and SrO and/or hydroxides PbOH or SrOH. The ionic packing density in a mineral's unit cell exerts a first-order control of their transport rates within the open space

Concluding remarks

A thorough compilation of experimentally determined diffusion data for Ar, H, Pb, and Sr has been used to test the general validity of empirical compensation relationships between activa-

tion energies and pre-exponential factors in silicate, carbonate, and phosphate minerals. Plotted as log$D$ vs. $10^3/T$, respective Arrhenius functions for diffusion of these elements in various minerals each converge at unique isokinetic temperatures (Fig. 12), at which all the diffusion rates are the same regardless of the diffusion mechanism, medium, and ionic porosity. Ionic porosity monitors ionic packing density in the unit cell of each mineral, and has been used in this study to systematize diffusion kinetics of elements at other temperatures in a wide array of minerals for which there are experimental data for comparison. On the basis of linear relationships of ionic porosity to activation energy (Ar and H diffusion), and to diffusivity at given temperatures (Pb and Sr diffusion), the diffusional activation energies and pre-exponential factors for these elements in various minerals have been estimated empirically from their calculated ionic porosities. Our calculated kinetics-porosity correlations compare favorably to existing experimental and/or other empirical data in most cases. A virtue of our kinetics-porosity modeling approach is that it allows diffusion coefficients to be predicted from crystal structures and ionic radii for minerals for which no experimental data currently exist. It will be a testament to the general robustness of this model if calculated diffusion coefficients are confirmed by subsequent experimental data and/or natural observations.

Treating minerals as a collection of more-or-less closely packed ionic spheres is clearly a simplification, and no theoretical basis has been established to explain the relationship between element diffusivity in minerals and their ionic porosities. Nonetheless, the first-order agreement between our empirical porosity-based estimates of diffusion parameters for various elements in diverse minerals, and with those determined experimentally by other researchers over a wide range of temperatures, is quite encouraging. Moreover, we have demonstrated that for most elements and minerals investigated, there is good adherence to a linear compensation relationship between diffusional activation energies and pre-exponential factors, especially if the occasional outlier is ignored.

Thus, it appears that the kinetics of elemental diffusion in minerals are largely rate-limited by the strength of chemical bonds, which vary systematically among minerals of different structures and composition, as monitored to a first approximation by their ionic porosities. Significantly, and as also noted above, our regressions can be used to make first-order predictions of diffusion coefficients in systems for which there are currently no experimental data, assuming that the compensation relation itself is not just an experimental artifact. To end on a cautionary note, however, uncertainty in the extent to which down-temperature extrapolations of experimental diffusion data (and differences therein) are valid at temperatures of geological interest stand as a practical limitation to the applicability of any empirical diffusion model to geothermometric and thermochronologic studies.

Acknowledgments

This study was supported by funds from the Natural Science Foundation of China (40573011 and 40334036) and the Chinese Academy of Sciences (KZCX3-SW-141). Thanks are due to J.B. Brady, P.S. Dahl, and an anonymous reviewer for their careful and constructive reviews, and to P.S. Dahl for his meticulous editorial handling of the work. We are also grateful to D.J. Cherniak, B.S. Kamber, F.J. Ryerson, I.M. Villa, and E.B. Watson for their insightful comments on earlier versions of this paper.

References cited

Baadsgaard, H., Lipson, J., and Folinsbee, R.E. (1961) The leakage of radiogenic argon from sanidine. Geochimica et Cosmochimica Acta, 25, 147–157.

Bejina, F. and Jaoul, O. (1997) Silicon diffusion in silicate minerals. Earth and Planetary Science Letters, 153, 229–238.

Berenov, A.V., MacManus-Driscoll, J.L., and Kilner, J.A. (2001) Observation of the compensation law during oxygen diffusion in perovskite materials. International Journal of Inorganic Materials, 3, 1109–1111.

Berry, L.G., Mason, B., and Dietrich, R.V. (1983) Mineralogy: Concepts, Descriptions, and Determinations, 561 p. W.H. Freeman and Company, San Francisco.

Blanchard, M. and Ingrin, J. (2004a) Kinetics of deuteration in pyrope. European Journal of Mineralogy, 16, 567–576.

——— (2004b) Hydrogen diffusion in Dora Maira pyrope. Physics and Chemistry of Minerals, 31, 593–605.

Bogolomov, Y. (1991) Migration of lead in non-metamict zircon. Earth and Planetary Science Letters, 107, 625–633.

Brabander, D.J. and Giletti, B.J. (1995) Strontium diffusion kinetics in amphiboles and significance to thermal history determinations. Geochimica et Cosmochimica Acta, 59, 2223–2238.

Brady, J.B. (1995) Diffusion data for silicate minerals, glasses, and liquids. In T.J. Ahrens, Ed., Mineral Physics and Crystallography, a Handbook of Physical Constants, 2, p. 269–290. American Geophysical Union, Reference Shelf, Washington, D.C.

Catlow, C.R.A. and Price, G.D. (1990) Computer modeling of solid-state inorganic materials. Nature, 347, 243–248.

Chakraborty, S., Farver, J.R., Yund, R.A., and Rubie, D.C. (1994) Mg tracer diffusion in synthetic forsterite and San Carlos olivine as a function of P, T and f_{O_2}. Physics and Chemistry of Minerals, 21, 489–500.

Chen, C.-H., DePaolo, D.J., and Lan, C.-Y. (1996) Rb-Sr microchrons in the Manaslu granite: implications for Himalayan thermochronology. Earth and Planetary Science Letters, 143, 125–135.

Cherniak, D.J. (1993) Lead diffusion in titanite and preliminary results on the effects of radiation damage on Pb transport. Chemical Geology, 110, 177–194.

——— (1995a) Diffusion of lead in plagioclase and K-feldspar: an investigation of Rutherford Backscattering and Resonant Nuclear Reaction Analysis. Contributions to Mineralogy and Petrology, 120, 358–371.

——— (1995b) Sr and Nd diffusion in titanite. Chemical Geology, 125, 219–232.

——— (1996) Strontium diffusion in sanidine and albite, and general comments on strontium diffusion in alkali feldspars. Geochimica et Cosmochimica Acta, 60, 5037–5043.

——— (1997) An experimental study of strontium and lead diffusion in calcite, and implications for carbonate diagenesis and metamorphism. Geochimica et Cosmochimica Acta, 61, 4173–4179.

——— (1998) Pb diffusion in clinopyroxene. Chemical Geology, 150, 105–117.

——— (2000) Pb diffusion in rutile. Contributions to Mineralogy and Petrology, 139, 198–207.

——— (2001) Pb diffusion in Cr diopside, augite, and enstatite, and consideration of the dependence of cation diffusion in pyroxene on oxygen fugacity. Chemical Geology, 177, 381–397.

——— (2006) Pb and rare earth element diffusion in xenotime. Lithos, 88, 1–14.

Cherniak, D.J. and Ryerson, F.J. (1993) A study of strontium diffusion in apatite using Rutherford backscattering and ion implantation. Geochimica et Cosmochimica Acta, 57, 4653–4662.

Cherniak, D.J. and Watson, E.B. (1992) A study of strontium diffusion in K-feldspar, Na-K feldspar, and anorthite using Rutherford Backscattering Spectroscopy. Earth and Planetary Science Letters, 113, 411–425.

——— (1994) A study of strontium diffusion in plagioclase using Rutherford backscattering spectroscopy. Geochimica et Cosmochimica Acta, 58, 5179–5190.

——— (2001) Pb diffusion in zircon. Chemical Geology, 172, 5–24.

——— (2003) Diffusion in zircon. In J.M. Hanchar and P.W.O. Hoskin, Eds., Zircon: Experiments, Isotopes, and Trace Element Investigations, 53, p. 113–143. Reviews in Mineralogy, Mineralogical Society of America, Chantilly, Virginia.

Cherniak, D.J., Lanford, W.A., and Ryerson, F.J. (1991) Lead diffusion in apatite and zircon using ion implantation and Rutherford backscattering techniques. Geochimica et Cosmochimica Acta, 55, 1663–1673.

Cherniak, D.J., Zhang, X.Y., Wayne, N.K., and Watson, E.B. (2001) Sr, Y, and REE diffusion in fluorite. Chemical Geology, 181, 99–111.

Cherniak, D.J., Watson, E.B., Grove, M., and Harrison, T.M. (2004) Pb diffusion in monazite: A combined RBS/SIMS study. Geochimica et Cosmochimica Acta, 68, 829–840.

Cole, D.R. and Chakraborty, S. (2001) Rates and mechanisms of isotopic exchange. In J.W. Valley, and D.R. Cole, Eds., Stable Isotope Geochemistry, 43, p. 83–223. Reviews in Mineralogy, Mineralogical Society of America, Chantilly, Virginia.

Connolly, C. and Muehlenbachs, K. (1988) Contrasting oxygen diffusion in nepheline, diopside, and other silicates and their relevance to isotopic systematics in meteorites. Geochimica et Cosmochimica Acta, 52, 1585–1591.
Coughlan, R.A.N. (1990) Studies in diffusion transport; grain boundary transport of oxygen in feldspars, strontium and the REE's in garnet, and thermal histories of granitic intrusions in south-central Maine using oxygen isotopes. Ph.D. dissertation, Brown University, Providence, Rhode Island.
Dahl, P.S. (1980) The compositional dependence of Fe^{2+}-Mg distributions between garnet and coexisting ferromagnesian silicates: applications to geothermometry. American Mineralogist, 65, 852–866.
——— (1996a) The effects of composition on retentivity of argon and oxygen in hornblende and related amphiboles: A field-tested empirical model. Geochimica et Cosmochimica Acta, 60(19), 3687–3700.
——— (1996b) The crystal-chemical basis for Ar retention in micas: inferences from interlayer partitioning and implications for geochronology. Contributions to Mineralogy and Petrology, 123, 22–39.
——— (1997) A crystal-chemical basis for Pb retention and fission-track annealing systematics in U-bearing minerals, with implications for geochronology. Earth and Planetary Science Letters, 150, 277–290.
Dahl, P.S., Pomfrey, M.E., and Foland, K.A. (2004) An $^{40}Ar/^{39}Ar$ study of post-tectonic cooling in the Adirondack Lowlands, Grenville Province, New York (U.S.A.), with implications for evolution of a major shear zone. Geological Society of America Memoir, 197 (Grenville Volume), 299–323.
De, S.K., Cole, D.R., Riciputi, L.R., Chacko, T., and Horita, J. (2000) Experimental determination of hydrogen diffusion rates in hydrous minerals using the ion microprobe. 10th V.M. Goldschmidt Conference Abstract, 5, 340.
Demouchy, S. and Mackwell, S. (2003) Water diffusion in synthetic iron-free forsterite. Physics and Chemistry of Minerals, 30, 486–494.
Dodson, M.H. (1973) Closure temperature in cooling geochronological and petrological systems. Contributions to Mineralogy and Petrology, 40, 259–274.
Dowty, E. (1980) Crystal-chemical factors affecting the mobility of ion in minerals. American Mineralogist, 65, 174–182.
Dyer, A. and Faghihian, H. (1998a) Diffusion in heteroionic zeolites: Part 1. Diffusion of water in heteroionic natrolites. Microporous and Mesoporous Materials, 21, 27–38.
——— (1998b) Diffusion in heteroionic zeolites: Part 2. Diffusion of water in heteroionic stilbites. Microporous and Mesoporous Materials 21, 39–44.
Dyer, A. and Molyneux, A. (1968) The mobility of water in zeolites-I. Self-diffusion of water in analcite. Journal of Inorganic Nuclear Chemistry, 30, 829–837.
Evernden, J.F., Curtis, G.H., Kistler, R.W., and Obradovich, J. (1960) Argon diffusion in glauconite, microcline, sanidine, leucite, and phlogopite. American Journal of Science, 258, 583–604.
Farver, J.R. and Giletti, B.J. (1989) Oxygen and strontium diffusion kinetics in apatite and their application to cooling rate determination. Geochimica et Cosmochimica Acta, 53, 1621–1631.
Foland, K.A. (1974) ^{40}Ar diffusion in homogeneous orthoclase and an interpretation of Ar diffusion in K-feldspars. Geochimica et Cosmochimica Acta, 38, 151–166.
Fortier, S.M. and Giletti, B.J. (1989) An empirical model for predicting diffusion coefficients in silicate minerals. Science, 245, 1481–1484
Freer, R. (1981) Diffusion in silicate minerals and glasses: A data digest and guide to the literature. Contributions to Mineralogy and Petrology, 76, 440–454.
Gaber, L.J., Foland, K.A., and Corbató, C.E. (1988) On the significance of argon release from biotite and amphibole during $^{40}Ar/^{39}Ar$ vacuum heating. Geochimica et Cosmochimica Acta, 52, 2457–2465.
Ganguly, J. (2002) Diffusion kinetics in minerals: Principles and applications to tectono-metamorphic processes. EMU Notes in Mineralogy, 4(10), 271–309.
Giletti, B.J. (1974) Studies in diffusion I: Ar in phlogopite mica, 634, p. 107–115. In A.W. Hofmann, B.J. Giletti, H.S. Yoder, Jr., and R.A. Yund, Eds., Geochemical Transport and Kinetics, 634. Carnegie Institute Publication, Washington, D.C.
——— (1991) Rb and Sr diffusion in alkali feldspars, with implications for cooling histories of rocks. Geochimica et Cosmochimica Acta, 55, 1331–1343.
Giletti, B.J. and Casserly, J.E.D. (1994) Sr diffusion kinetics in plagioclase feldspars. Geochimica et Cosmochimica Acta, 58, 3785–3793.
Giletti, B.J. and Tullis, J. (1977) Studies in diffusion, IV. Pressure dependence of Ar diffusion in phlogopite mica. Earth and Planetary Science Letters, 35, 180–183.
Graham, C.M. (1981) Experimental hydrogen isotope studies: III. Diffusion of hydrogen in hydrous minerals, and stable isotope exchange in metamorphic rocks. Contributions to Mineralogy and Petrology, 76, 216–228.
Graham, C.M., Sheppard, S.M.F., and Heaton, T.H.E. (1980) Experiment hydrogen isotope studies I. Studies of hydrogen isotope fractionation in the systems epidote-H_2O, zoisite-H_2O, and AlO(OH)-H_2O. Geochimica et Cosmochimica Acta, 44, 353–364.
Graham, C.M., Harmon, R.S., and Sheppard, S.M.F. (1984) Experimental hydrogen isotope studies: Hydrogen isotope exchange between amphibole and water. American Mineralogist, 69, 128–138.
Graham, C.M., Viglino, J.A., and Harmon, R.S. (1987) Experimental study of hydrogen- isotope exchange between aluminous chlorite and water and of hydrogen diffusion in chlorite. American Mineralogist, 72, 566–579.
Grove, M. and Harrison, T.M. (1996) $^{40}Ar^*$ diffusion in Fe-rich biotite. American Mineralogist, 81, 940–951.
Guo, J.B. and Qian, Y.Q. (1997) Hydrogen isotope fractionation and hydrogen diffusion in the tourmaline-water system. Geochimica et Cosmochimica Acta, 61, 4679–4688.
Hames, W.E. and Bowring, S.A. (1994) An empirical evaluation of argon diffusion geometry in muscovite. Earth and Planetary Science Letters, 124, 161–169.
Hammouda, T. and Cherniak, D.J. (2000) Diffusion of Sr in fluorphlogopite determined by Rutherford backscattering spectrometry. Earth and Planetary Science Letters, 178, 339–349.
Hariya, Y. and Tsutusmi, M. (1981) Hydrogen isotopic composition of MO(OH) minerals from manganess oxide and massive sulfide (Kuroko) deposit in Japan. Contributions to Mineralogy and Petrology, 77, 256–261.
Harrison, T.M. (1981) Diffusion of ^{40}Ar in hornblende. Contributions to Mineralogy and Petrology, 78, 324–331.
Harrison, T.M., Duncan, I., and McDougall, I. (1985) Diffusion of ^{40}Ar in biotite: Temperature, pressure, and compositional effects. Geochimica et Cosmochimica Acta, 49, 2461–2468.
Hart, S.R. (1981) Diffusion compensation in natural silicates. Geochimica et Cosmochimica Acta, 45, 279–291.
Hercule, S. and Ingrin, J. (1999) Hydrogen in diopside: Diffusion, kinetics of extraction-incorporation, and solubility. American Mineralogist, 84, 1577–1587.
Hofmann, A.W. (1980) Diffusion in natural silicate melts: A critical review. In R. Hargraves, Ed., Physics of Magmatic Processes, p. 385–417. Princeton University Press, New Jersey.
Ingrin, J., Hercule, S., and Charton, T. (1995) Diffusion of hydrogen in diopside: Results of dehydration experiments. Journal of Geophysical Research, 100(B8), 15489–15499.
Ita, J. and Cohen, R.E. (1997) Effects of pressure on diffusion and vacancy formation in MgO from nonempirical free-energy integrations. Physics Review Letter, 79(17), 3198–3201.
Jaoul, O. and Bejina, F. (2005) Empirical determination of diffusion coefficients and geospeedometry. Geochimica et Cosmochimica Acta, 69, 1027–1040.
Jenkin, G.R.T. (1997) Do cooling paths derived from mica Rb-Sr data reflect true cooling paths? Geology, 25(10), 907–910.
Johnson, O.W., Paek, S.H., and Deford, J.W. (1975) Diffusion of H and D in TiO_2: Suppression of internal fields by isotope exchange. Journal of Applied Physics, 46, 1026–1033.
Kamber, B.S., Blenkinsop, T.G., Villa, I.M., and Dahl, P.S. (1995) Proterozoic transpressive deformation in the Northern Marginal Zone, Limpopo Belt, Zimbabwe. Journal of Geology, 103, 493–508.
Kats, A., Haven, Y., and Stevels, J.M. (1962) Hydroxyl groups in β-quartz. Physics and Chemistry of Glasses, 3, 69–75.
Kemeny, G. and Rosenberg, B. (1973) Compensation law in thermodynamics and thermal death. Nature, 243, 400.
Kischner, D.L., Cosca, M.A., Masson, H., and Hunziker, J.C. (1996) Staircase $^{40}Ar/^{39}Ar$ spectra of the fine-grained white mica: timing and duration of deformation and empirical constraints on argon diffusion. Geology, 24, 747–750.
Kronenberg, A.K., Kirby, S.H., Aines, R.D., and Rossman, G.R. (1986) Solubility and diffusional uptake of hydrogen in quartz at high water pressures: implications for hydrolytic weakening. Journal of Geophysical Research, 91, 12723–12744.
Kronenberg, A.K., Yund, R.A., and Rossman, G.R. (1996) Stationary and mobile hydrogen defects in potassium feldspar. Geochimica et Cosmochimica Acta, 60(21), 4075–4094.
Lasaga, A.C. (1998) Kinetic Theory in the Earth Sciences, 811 p. Princeton University Press, New Jersey.
Lee, J.K.W., Williams, I.S., and David, J.E. (1997) Pb, U, and Th diffusion in natural zircon. Nature, 39, 159–162.
Liu, K.K. and Epstein, S. (1984) The hydrogen isotope fractionation between kaolinite and water. Chemical Geology, 2, 335–350.
Mackwell, S.J. and Kohlstedt, D.L. (1990) Diffusion of Hydrogen in Olivine: Implications for Water in the Mantle. Journal of Geophysical Research, 95(84), 5079–5088.
Magomedov, S.A. (1970) Migration of radiogenic products in zircon. Geokhimiya, 2, 263–267 (in Russian).
Misra, N.K. and Venkatasubramanian, V.S. (1977) Strontium diffusion in feldspars: a laboratory study. Geochimica et Cosmochimica Acta, 41, 837–838.
Moore, D.K., Cherniak, D.J., and Watson, E.B. (1998) Oxygen diffusion in rutile from 750 to 1000 °C and 0.1 to 1000 MPa. American Mineralogist, 83, 700–711.
Morioka, M. and Nagasawa, H. (1991) Diffusion in single crystals of melilite: II. Cations. Geochimica et Cosmochimica Acta, 55, 751–759.
Morishita, Y., Giletti, B.J., and Farver, J.R. (1990) Strontium and oxygen self-diffusion in titanite. Eos Transaction American Geophysics Union, 71, 652.
Muehlenbachs, K. and Connolly, C. (1991) Oxygen diffusion in leucite: Structural

controls. In H.P. Taylor, Jr., J.R. O'Neil, and I.R. Kaplan, Eds., Stable Isotope Geochemistry: A Tribute to Samuel Epstein, 3, 27–34. Geochemical Society Special Publication.

O'Neil, J.R. and Kharaka, Y.K. (1976) Hydrogen and oxygen isotope exchange between clay minerals and waters. Geochimica et Cosmochimica Acta, 40, 241–246.

Patel, A., Price, G.D., and Mendelssohn, M.J. (1991) A computer simulation approach to modeling the structure, thermodynamics, and oxygen isotope equilibria of silicates. Physics and Chemistry of Minerals, 17, 690–699.

Peck, W.H., Valley, J.W., and Graham, C.M. (2003) Slow oxygen diffusion rates in igneous zircons from metamorphic rocks. American Mineralogist, 88, 1003–1014.

Purton, J. and Catlow, C.R.A. (1990) Computer simulation of feldspar structures. American Mineralogist, 75, 1268–1273.

Qian, Y.Q. and Guo, J.B. (1993) Study of hydrogen isotope equilibrium and kinetic fractionation in the ilvaite-water system. Geochimica et Cosmochimica Acta, 57, 3073–3082.

Ramirez, R., Gonzatez, R., Colera, I., and Chen, Y. (1997) Diffusion of deuterons and protons in α-Al_2O_3 crystals enhanced by an electric field. Material Science Forum, 239–241, 395–398.

Reynolds, J.H. (1957) Comparative study of argon content and argon diffusion in mica and feldspar. Geochimica et Cosmochimica Acta, 12, 177–184.

Robbins, G.A. (1972) Radiogenic argon diffusion in muscovite under hydrothermal conditions. M.S. thesis, Brown University, Providence, Rhode Island.

Rosenqvist, I.Th. (1949) Some investigations in the crystal chemistry of silicates. 1. Diffusion of Pb and Ra in feldspar. Acta Chemica Scandinavica, 3, 569–583.

Sakai, H. and Tsutsumi, M. (1978) D/H fractionation factor between serpentine and water at 100 to 500 °C and 2000 bars water pressure, and the D/H ratios of natural serpentine. Earth and Planetary Science Letters, 40, 231–242.

Scott, D.J. and St-Onge, M.R. (1995) Constraints on Pb closure temperature in titanite based on rocks from the Ungava orogen, Canada: Implications for U-Pb geochronology and *P-T-t* path determinations. Geology, 23, 1123–1126.

Shaffer, E.W., Sang, S-L.J., Cooper, A.R., and Heuer, A.H. (1974) Diffusion of tritiated water in β-quartz. In A.W. Hofmann, B.J. Giletti, H.S. Yoder, Jr., and R.A. Yund, Eds., Geochemical kinetics and transport, 634, p. 131–138. Carnegie Institute Publication, Washington, D.C.

Shannon, R.D. (1976) Revised effective ionic radii and systematic studies of interatomic distances in halides and chalcogenides. Acta Crystallographica, A32, 751–767.

Shannon, R.D. and Prewitt, C.T. (1969) Effective ionic radii in oxides and fluorides. Acta Crystallographica, B25, 925–945.

Shestakov, G.I. (1969) On diffusional loss of lead from a radioactive mineral. Geochemistry International, 6, 888–896.

——— (1972) Diffusion of lead in monazite, zircon, sphene, and apatite. Geochemistry International, 9, 801–807.

Shuster, D.L. and Farley, K.A. (2005) Diffusion kinetics of proto-induced ^{21}Ne, ^{3}He, and ^{4}He in quartz. Geochimica et Cosmochimica Acta, 69, 2349–2359.

Smith, H.A. and Giletti, B.J. (1997) Lead diffusion in monazite. Geochimica et Cosmochimica Acta, 61, 1047–1055.

Smyth, J.R. and Bish, D.L. (1988) Crystal Structures and Cation Sites of the Rock-Forming Minerals, 332 p. Allen and Unwin, Boston.

Sneeringer, M., Hart, S.R., and Shimizu, N. (1984) Strontium and samarium diffusion in diopside. Geochimica et Cosmochimica Acta, 48, 1589–1608.

Stalder, R. and Skogby, H. (2003) Hydrogen diffusion in natural and synthetic orthopyroxene. Physics and Chemistry of Minerals, 30, 12–19.

Stoffregen, R.E., Rye, T.O., and Wasserman, M.D. (1994) Experimental studies of alunite: II. Rates of alunite-water alkali and isotope exchange. Geochimica et Cosmochimica Acta, 58, 917–929.

Suzuoki, T. and Epstein, S. (1976) Hydrogen isotope fractionation between OH-bearing minerals and water. Geochimica et Cosmochimica Acta, 40, 1229–1240.

Van Orman, J.A., Fei, Y.W., Hauri, E.H., and Wang, J.H. (2003) Diffusion in MgO at high pressures: constraints on deformation mechanisms and chemical transport at the core-mantle boundary. Geophysical Research Letters, 30(2), 1056, DOI: 10.1029/2002GL016343.

Vennemann, T.W., O'Neil, J.R., Deloule, E., and Chaussidon, M. (1996) Mechanism of hydrogen isotope exchange between hydrous minerals and molecular hydrogen: Ion microprobe study of D/H exchange and calculations of hydrogen self-diffusion rates. Abstracts of the 6th VM Goldschmidt Conference, Heidelberg, 648.

Villa, I.M. (1998) Isotopic closure. Terra Nova, 10, 42–47.

——— (2006) From nanometer to megameter: Isotopes, atomic-scale processes, and continent-scale tectonic models. Lithos, 87, 155–173.

Villa, I.M. and Puxeddu, M. (1994) Geochronology of the Larderello geothermal field: new data and the "closure temperature" issue. Contributions to Mineralogy and Petrology, 115, 415–426.

Villa, I.M., Grobety, B., Kelley, S.P., Trigila, R., and Wieler, R. (1996) Assessing Ar transport paths and mechanisms in the MaClure Mountains hornblende. Contributions to Mineralogy and Petrology, 126, 67–80.

Vocadlo, L., Wall, A., Parker, S.C., and Price, G.D. (1995) Absolute ionic diffusion in MgO-computer calculations via lattice dynamics. Physics of Earth Planetary Interior, 88, 193–210.

Voltaggio, M. (1985) Estimation of diffusion constants by observations of isokinetic effects: A test for radiogenic argon and strontium. Geochimica et Cosmochimica Acta, 49, 2117–2122.

Walker, A.M., Wright, K., and Slater, B. (2003) A computational study of oxygen diffusion in olivine. Physics and Chemistry of Minerals, 30, 536–545.

Wang, L.P., Zhang, Y.X., and Essene, E.J. (1996) Diffusion of the hydrous component in pyrope. American Mineralogist, 81, 706–718.

Wartho, J.-A., Kelley, S.P., Brooker, R.A., Carroll, M.R., Villa, I.M., and Lee, M.R. (1999) Direct measurement of Ar diffusion profiles in a gem-quality Madagascar K-feldspar using the ultra-violet laser ablation microprobe (UVLAMP). Earth and Planetary Science Letters, 170, 141–153.

Watson, E.B. and Cherniak, D.J. (2003) Lattice diffusion of Ar in quartz, with constraints on Ar solubility and evidence of nanopores. Geochimica et Cosmochimica Acta, 67, 2043–2062.

Watson, E.B., Harrison, T.M., and Ryerson, F.J. (1985) Diffusion of Sm, Ar, and Pb in fluorapatite. Geochimica et Cosmochimica Acta, 49, 1813–1823.

Winchell, P. (1969) The compensation law for diffusion in silicates. High Temperature Science, 1, 200–215.

Winchell, P. and Norman, J.H. (1969) A study of the diffusion of radioactive nuclides in molten silicates at high temperatures.3rd International Symposium on High Temperature Technology, Pure Applied Chemistry, Supplement, 479–492.

Woods, S.C., Mackwell, S., and Dyar, D. (2000) Hydrogen in diopside: Diffusion profiles. American Mineralogist, 85, 480–487.

Wright, K. and Catlow, C.R.A. (1994) A computer simulation of OH defects in olivine. Physics and Chemistry of Minerals, 20, 515–518.

Wright, K., Freer, R., and Catlow, C.R.A. (1995) Oxygen diffusion in grossular and some geological implications. American Mineralogist, 80, 1020–1025.

——— (1996) Water-related defects and oxygen diffusion in albite: a computer simulation study. Contributions to Mineralogy and Petrology, 125, 161–166.

Yang, M.H. and Flynn, C.P. (1994) Intrinsic diffusion properties of an oxide: MgO. Physics Review Letter, 73(13), 1809–1812.

Zheng, Y.-F. and Fu, B. (1998) Estimation of oxygen diffusivity from anion porosity in minerals. Geochemical Journal, 32, 71–89.

Zheng, Y.-F., Zhao, Z.-F., Li, S.G., and Gong, B. (2003) Oxygen isotope equilibrium between ultrahigh-pressure metamorphic minerals and its constraints on Sm-Nd and Rb-Sr chronometers. In D. Vance, W. Muller, and I. Villa, Eds., Geochronology: Linking the Isotope Record with Petrology and Textures. Geological Society Special Publications, 220, 93–117.

MANUSCRIPT RECEIVED OCTOBER 25, 2005
MANUSCRIPT ACCEPTED OCTOBER 3, 2006
MANUSCRIPT HANDLED BY PETER DAHL